PALEOECOLOGY

Global acceleration in rates of vegetation change over the past 18,000 years

Ondřej Mottl[1]*†, Suzette G. A. Flantua[1,2]*†, Kuber P. Bhatta[1], Vivian A. Felde[1,2], Thomas Giesecke[3], Simon Goring[4,5], Eric C. Grimm[6]‡, Simon Haberle[7,8], Henry Hooghiemstra[9], Sarah Ivory[10], Petr Kuneš[11], Steffen Wolters[12], Alistair W. R. Seddon[1,2], John W. Williams[4,5]

Global vegetation over the past 18,000 years has been transformed first by the climate changes that accompanied the last deglaciation and again by increasing human pressures; however, the magnitude and patterns of rates of vegetation change are poorly understood globally. Using a compilation of 1181 fossil pollen sequences and newly developed statistical methods, we detect a worldwide acceleration in the rates of vegetation compositional change beginning between 4.6 and 2.9 thousand years ago that is globally unprecedented over the past 18,000 years in both magnitude and extent. Late Holocene rates of change equal or exceed the deglacial rates for all continents, which suggests that the scale of human effects on terrestrial ecosystems exceeds even the climate-driven transformations of the last deglaciation. The acceleration of biodiversity change demonstrated in ecological datasets from the past century began millennia ago.

One of the clearest forms of biodiversity change during the past century has been the increased rates of species turnover across the marine and terrestrial biospheres (*1*–*3*). Today, >75% of Earth's ice-free land surface has been altered by human land use (*4*), with profound effects on the composition and functioning of ecosystems. Globally, extinction rates are increasing (*5*), although trends in local species richness are ambiguous (*6*).

These increased rates of species turnover, as signified by local and regional changes in community composition, are embedded in a longer-term context in which humanity's footprint has steadily grown since humans first began to alter landscapes for food, energy, and other resources. Hominid use of fire began at least 700,000 years ago (*7*), low-intensity but extensive agricultural land use began ~8000 years ago, and intensive agricultural land use expanded after 6000 years ago (*8*) (Fig. 1B). Detectable human imprints on vegetation began thousands of years ago (*9*, *10*), and the composition and carbon sequestration of many contemporary ecosystems remain profoundly influenced by the legacies of anthropogenic land use over the past centuries to millennia (*11*). Nonetheless, there remains a notable knowledge and scale gap between contemporary studies of global biodiversity trends of the past century (*2*) and studies examining early anthropogenic effects on ecosystems. Observational syntheses of global biodiversity trends are limited to the past several centuries, whereas macroscale syntheses of vegetation changes from fossil pollen data have been limited to continental scales (*9*) or are largely qualitative (*12*). Consequently, global patterns and magnitudes of vegetation compositional change, which are important for understanding how biodiversity and ecosystem dynamics have been shaped by climate change and early human activity, are poorly understood.

In parallel, paleoecological studies have shown the high sensitivity of terrestrial ecosystems to the climate changes that accompanied and followed the last deglaciation [~20,000 to 8200 calibrated years before radiocarbon present (cal yr BP, where 0 yr BP is 1950 CE); 20 to 8.2 thousand calibrated years BP (ka); Fig. 1, C and D] (*12*, *13*). In temperate and boreal regions, forest expanded from glacial refugia as temperatures rose and precipitation patterns shifted, with widespread leading-edge range expansions and, for some taxa, trailing-edge range contractions (*14*). Novel ecosystems emerged in response to novel climates and the Late Pleistocene extinction of megaherbivores (*15*). Tropical and subtropical ecosystems responded to rising temperatures linked to increasing greenhouse gases (Fig. 1D) and hydrological shifts driven by precessional controls on monsoons and the Intertropical Convergence Zone (*16*). Consequently, during the Pleistocene-Holocene transition, tropical ecosystems substantially changed in species composition and canopy structures across all elevations (*17*), whereas millennial- and centennial-scale hydroclimate variability caused abrupt changes in global vegetation during the Holocene (*18*).

Ecosystem responses to humans and climate change over long time scales can now be assessed globally, thanks to the century-long expansion of a global network of fossil pollen sequences anchored by increasingly precise radiocarbon chronologies (*19*); the building of open, community-curated data resources (*20*); and the development of new rate-of-change techniques (*21*). Here, we assess the global patterns and rates of vegetation change from the last deglaciation, through the Holocene, and up to the current Anthropocene on the basis of 1181 fossil pollen sequences from the Neotoma Paleoecology Database (*20*) covering all continents except Antarctica (Fig. 1 and data S1). These analyses are based on continentally harmonized taxonomies and updated Bayesian chronologies with age-depth model uncertainties and an improved algorithm [R package *R-Ratepol*; (*21*, *22*)] for estimating rates of change (RoCs) for paleoecological time series. RoCs are calculated as the compositional dissimilarity between consecutive time intervals (using the chi-squared coefficient) standardized by the length of time between samples, thereby providing an indicator of compositional change per unit of time. *R-Ratepol* uses a moving-window approach (instead of the traditional calculation of dissimilarities between individual levels), which minimizes artifactual alterations in RoC resulting from variations in sample density and sedimentation rate (*21*). *R-Ratepol* also incorporates temporal uncertainty resulting from age-depth modeling calculations through randomization (*21*, *22*). For each pollen sequence, we pooled data into 500-year time bins [see also our 250-year sensitivity experiment in the supplementary materials (*22*)] and calculated RoCs between bins to represent the rate of compositional change through time. For each sequence, we also identified time intervals with a large increase in RoC, called peak points [for more detailed information, see materials and methods (*22*)].

We analyzed RoCs at the scale of continents and subcontinental clusters, defined by climatic and geographic variables (*22*). For each continent and subcontinental region, we binned the RoC scores per 500-year time bins [with a 250-year sensitivity experiment in the supplementary materials (*22*)] and calculated the 95% RoC quantile to highlight intervals and places with large vegetation changes while filtering out outliers [see (*22*) for a comparison of the 95% quantile to median trends]. Similarly, we calculated the proportion of sequences with a peak point in each time bin. The clustering of peak points among sequences indicates a synchronous period of abrupt vegetation change within a region. Generalized additive models were fitted to all RoCs and peak point curves to

[1]Department of Biological Sciences, University of Bergen, N-5020 Bergen, Norway. [2]Bjerknes Centre for Climate Research, University of Bergen, N-5020 Bergen, Norway. [3]Department of Physical Geography, Utrecht University, 3508 TC, Utrecht, Netherlands. [4]Department of Geography, University of Wisconsin-Madison, Madison, WI, USA. [5]Center for Climatic Research, University of Wisconsin-Madison, Madison, WI, USA. [6]Department of Earth and Environmental Sciences, University of Minnesota, Minneapolis, MN, USA. [7]Department of Archaeology and Natural History, Australian National University, Canberra, ACT 2601, Australia. [8]Australian Research Council Centre of Excellence in Australian Biodiversity and Heritage, Australian National University, Canberra, ACT 2601, Australia. [9]Department of Ecosystem and Landscape Dynamics, University of Amsterdam, 1098 XH, Amsterdam, Netherlands. [10]Department of Geosciences and the Earth and Environmental Systems Institute (EESI), Penn State University, University Park, PA, USA. [11]Department of Botany, Faculty of Science, Charles University, Prague, Czech Republic. [12]Lower Saxony Institute for Historical Coastal Research, Wilhelmshaven, Germany.
***Corresponding author. Email: ondrej.mottl@gmail.com (O.M.); s.g.a.flantua@gmail.com (S.G.A.F.)**
†These authors contributed equally to this work.
‡Deceased.

summarize trends and test for significant accelerations [simultaneous confidence intervals of the first derivative differ from zero (*22*)].

We detect an unequivocal global acceleration of vegetation change during the Late Holocene (4.2 to 0 ka; Fig. 2). The estimated start of acceleration differs among continents and ranges from 4.6 to 3.1 ka (table S1). This estimated start is well supported by the dense availability of samples during the Middle to Late Holocene (Fig. 1E), but continental-scale estimates vary by ~500 to 1000 years (*22*). For most continents, Late Holocene RoCs are close to or exceed RoCs over the past 18 ka, with a percent differential ranging from −6.3 to 22.2% (Fig. 2 and table S1). Increases in RoC during the Lateglacial and Early Holocene can be linked to temperature and atmospheric CO_2 variations (Fig. 1, C and D) and hydrological variations. Rapid vegetation changes concentrate near the onset of the Holocene (11.7 ka) for most continents, expressed as a maximum in RoC or in peak points (Fig. 2). In North America and Europe, RoCs reached maxima during the abrupt millennial-scale climate oscillations characteristic of the North Atlantic and adjacent regions (~15 to 11 ka) and then substantially declined during the Early Holocene (Fig. 2, A and B). The heightened rates of deglacial vegetation change resemble the patterns of increased temperature variability in the North Atlantic and elsewhere in the Northern Hemisphere that were driven by a combination of orbital forcing, atmospheric greenhouse gas concentrations, meltwater pulses to the North Atlantic, and shifting patterns of heat transport (*23*). In Asia, rapid but asynchronous change characterizes the Lateglacial and deglaciation period, with a maximum in RoCs or a clustering

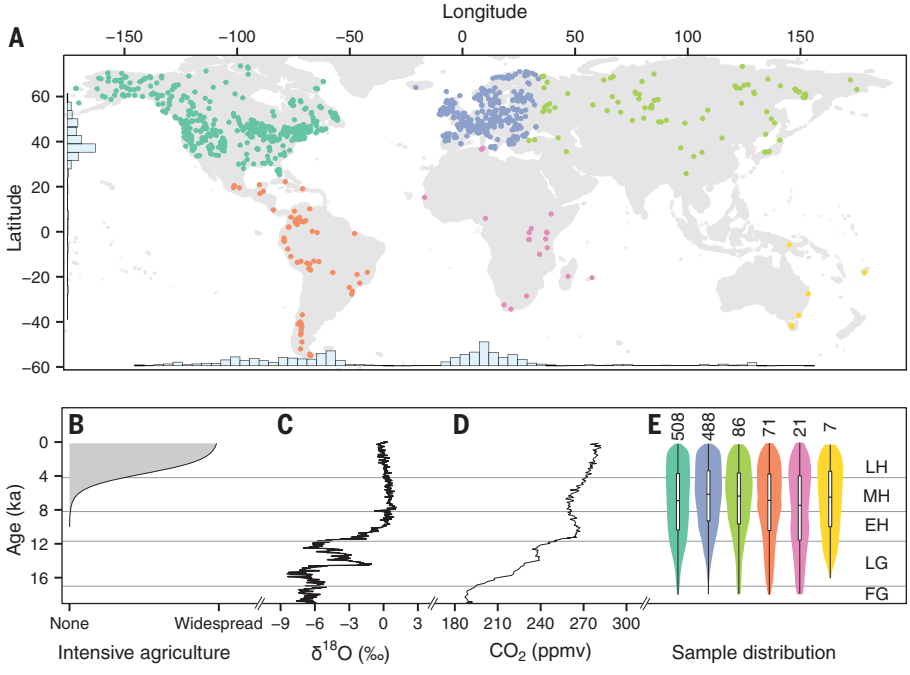

Fig. 1. Spatiotemporal distribution of the fossil pollen sequences analyzed here and climate and anthropogenic changes during the past 18,000 years. (**A**) Spatial distribution of pollen sequences used in this work. Histograms indicate the frequency of sequences across longitude and latitude. (**B**) Development of intensive agriculture based on archaeological expert elicitation (*8*). (**C**) $\delta^{18}O$, a temperature proxy, from the North Greenland Ice Core Project (NGRIP) (*38*). ‰, per mil. (**D**) Atmospheric CO_2 concentration [EPICA DOME C (*39*)]. ppmv, parts per million volume. (**E**) The number of pollen sequences per continent [colors match those in (A)] and sample density over the studied period. FG, full glacial; LG, Lateglacial; EH, Early Holocene; MH, Middle Holocene; LH, Late Holocene.

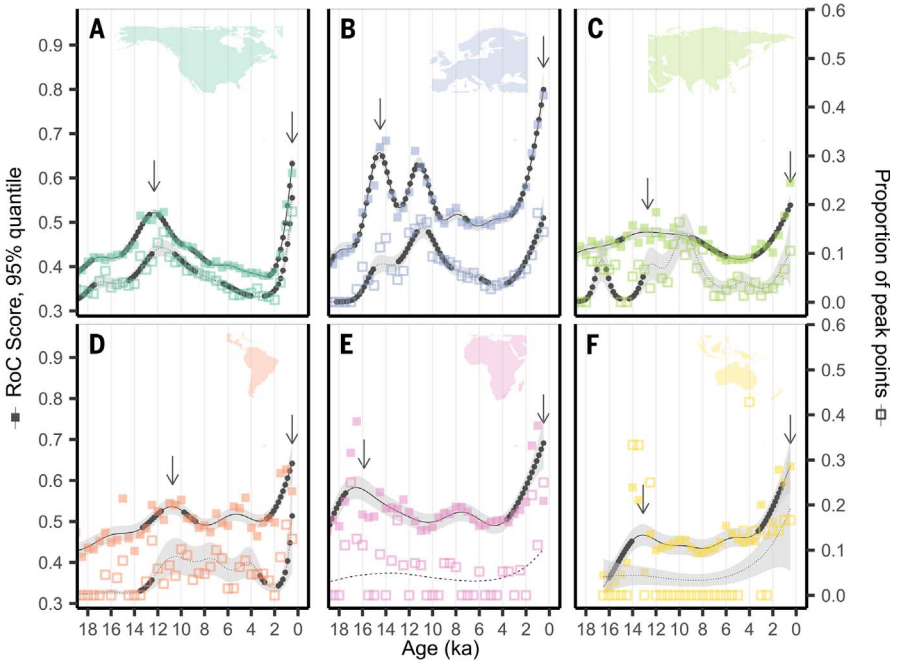

Fig. 2. RoC analyses by continent. (**A** to **F**) The filled squares represent the upper 95% quantile RoC score (left *y* axis) per 500-year time bin, with the solid curve representing the corresponding generalized additive model (GAM) (*22*). High values indicate high rates of vegetation change. Empty squares represent the proportion of peak points within each time bin (right *y* axis), with the corresponding GAM curve indicated by a dotted line. High values indicate a high synchrony in RoC among sequences (*22*). When the relationship is not significant, the GAM line is shown as dashed, and the error envelope is absent. Black asterisks on the GAM curves identify periods of significant acceleration in vegetation RoCs (i.e., where the derivative significantly differs from zero). Arrows indicate maximum RoC values for the Late Holocene and the Pleistocene-Holocene transition (table S1).

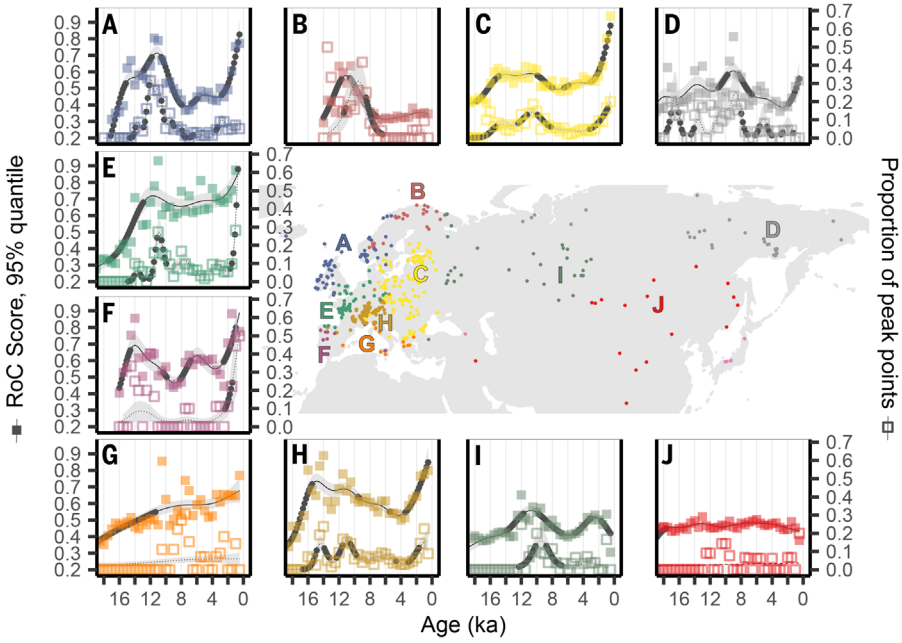

Fig. 3. RoC analyses by region across Eurasia. (**A** to **J**) Figure design follows that of Fig. 2.

of peak points between 10 and 8 ka (Fig. 2C). In Latin America and Africa, RoCs also reach maxima between 10 and 8 ka, which can be linked to altered monsoonal rainfall associated with declining Northern Hemisphere summer insolation (*24*).

RoC patterns at subcontinental scales are consistent with known histories of climate change and human land use. For example, in Eurasia, the western and northern European clusters show strong peaks in the rate of vegetation change between 15 and 10 ka (Fig. 3, A and E), which is consistent with the response of vegetation to North Atlantic climate variations and the retreating Eurasian ice sheets (Fig. 1C). Late Holocene rates of vegetation change are high across western and central Europe, particularly in areas of high present and past agricultural activity (*10*). In Asia, high rates of vegetation change during the Early Holocene can be linked to postglacial forest expansion in northern Asia (*25*) and millennial-scale variability in temperature and monsoonal rainfall in eastern Asia (*26*) (Fig. 3, C, D, and I). Seven of 10 Eurasian clusters show increased RoCs during the Late Holocene.

In the Americas, vegetation RoCs vary by latitude and between Atlantic- and Pacific-adjacent regions (Fig. 4). Eastern North America resembles western Europe in its high vegetation RoCs between 15 and 10 ka, with a strong signal of synchronous vegetation change over the past millennium (Fig. 4, G, H, and I). All North American regions show increased RoCs during the Late Holocene except for the high-latitude clusters. Driven by the topographic complexity of the Andes, vegetation responses in the Neotropical highlands were highly variable and asynchronous (Fig. 4D)—likely a combined effect of changes in temperature, hydroclimate variability, and atmospheric CO_2 (*27*, *28*). In the lowlands, a peak in vegetation RoCs at 10 ka is likely the result of hydrological variability linked to shifting monsoons (Fig. 4J) (*27*). These large vegetation changes challenge the common myth of the stable tropics and suggest a strong sensitivity of the Neotropics to temperature, hydroclimate variability, and orbital precession during the Early Holocene (*27*, *28*). In temperate South America, a period of synchronous vegetation change in the Holocene (Fig. 4E) is asynchronous with warm Neotropical regions (Fig. 4J), likely because of varying climate modes influencing different parts of the continent (*29*). The Late Holocene acceleration of vegetation change is clearly manifested across most of the latitudinal gradient of the Americas, except for the high northern latitudes, with the highest RoCs in coastal western North America and eastern North America (Fig. 4).

The detection of globally accelerating rates of vegetation change during the Late Holocene provides a longer-term perspective to the well-documented increase in species turnover during the 20th and 21st centuries (*6*). For terrestrial ecosystems at least, these recent increases in species turnover are the continuation of a longer acceleration that began millennia ago (Fig. 2). Moreover, this work suggests that contemporary communities and some current biodiversity trends may be partially resulting from legacies of past land use or environmental forcing (*11*) in combination with the strong anthropogenic imprint of the past decades. Hence, recent changes in biodiversity patterns represent only the most recent interval of our used planet (*30*) that has been altered by millennia of changing environments and human activities.

Our study focused primarily on detecting patterns of rates of vegetation compositional changes over the past 18,000 years and secondarily on attributing causes. This approach follows the standard delineation in climate change research between detection studies that focus on establishing the significance and fingerprints of observed climate trends (*31*) and attribution studies that explore the potential causes of the observed events and patterns (*32*). Biodiversity research is now achieving the capability for global detection analyses (*2*, *6*) across an increasingly broad range of time scales. The next frontier is to disentangle and attribute the contributions of climatic variability and anthropogenic impacts to past vegetation changes. This attribution is challenged by the complex interplay between climatic, anthropogenic, and vegetation dynamics that varies within and among ecosystems, particularly at local to regional scales. For example, in the Holocene in East Africa, land cover changes over the past 6000 years were driven by multiple cultural and technological innovations and by changes in rainfall amount and seasonality (*33*). In South America, Holocene climate variability contributed to regime shifts in human demography and displacement, which in turn affected ecosystems regionally (*34*). The worldwide spread of agricultural land use over the past 3000 years suggests intensified resource management (*8*) but was accompanied in some regions by substantial climate changes (*16*, *33*). Deglacial vegetation dynamics, although strongly climate driven, were also affected by global megaherbivore extinctions during the late Quaternary (*15*), which likely resulted from synergistic anthropogenic and climatic drivers (*35*). These interactions provide evidence against single-cause attributions of rates of vegetation change.

A key next step is to integrate these paleovegetation sequences with other paleoclimatic and archaeological records to better understand the past feedbacks among the climate, ecosystems, and humans (*3*, *10*, *13*, *36*) and the legacy effects of these past interactions on the trajectory of contemporary ecosystems. Assembled networks of paleovegetation, paleoclimatic, and anthropogenic records need to be harmonized and quality checked to do this attribution correctly and handle the spatial variations in vegetation, climate, and human histories within and among continents (*36*). Such an integration will also need carefully chosen numerical techniques to formally detect the onset of detectable human influence in paleoenvironmental time series and the variation in timing within and among ecosystems (*29*). Additionally, a higher density of paleoecological records is still needed, especially in topographically rich regions such as

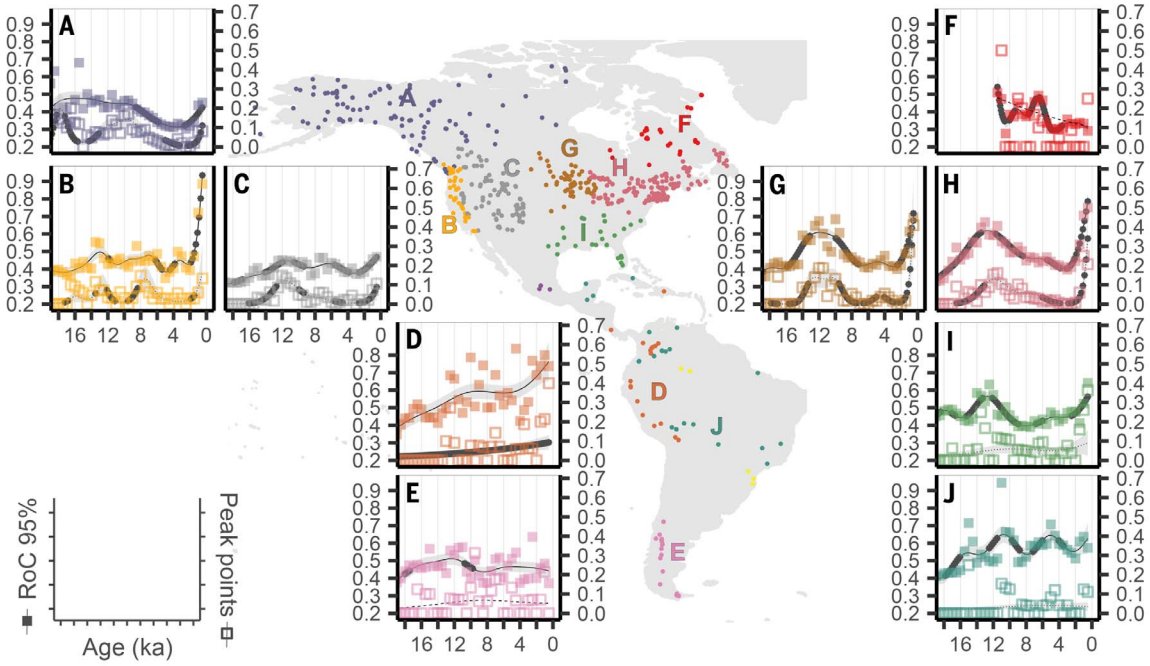

Fig. 4. RoC analyses by region across the Americas. (**A** to **J**) Figure design follows that of Fig. 2.

the Himalayas and the Andes, where climate heterogeneity is highest and human activities span millennia.

Despite these complexities, it is well known that the mean global temperature increases during the last deglaciation (~6°C) were several times as large as those of the Middle to Late Holocene [~1°C (*37*)]. Thus, a reasonable working inference is that the globally enhanced rates of vegetation change over the past several thousand years were caused primarily by anthropogenic activities, whereas vegetation changes during the Late Pleistocene to Early Holocene were driven primarily by changing climates. If so, the magnitude and extent of Late Holocene rates of vegetation change suggests that the global transformation of the terrestrial biosphere by humans now resembles or exceeds in rate and scope even the profound ecosystem transitions associated with the end of the last glacial period. Moreover, the global ecosystem changes for this century may be greater yet given current climate commitments and given that the climate changes expected for higher-end emission scenarios are similar in magnitude to those of the last deglaciation.

REFERENCES AND NOTES

1. B. J. McGill, M. Dornelas, N. J. Gotelli, A. E. Magurran, *Trends Ecol. Evol.* **30**, 104–113 (2015).
2. M. Dornelas *et al.*, *Glob. Ecol. Biogeogr.* **27**, 760–786 (2018).
3. J. Woodbridge *et al.*, *J. Ecol.* **109**, 1396–1410 (2021).
4. E. C. Ellis, N. Ramankutty, *Front. Ecol. Environ.* **6**, 439–447 (2008).
5. S. L. Pimm *et al.*, *Science* **344**, 1246752 (2014).
6. S. A. Blowes *et al.*, *Science* **366**, 339–345 (2019).
7. D. M. J. S. Bowman *et al.*, *J. Biogeogr.* **38**, 2223–2236 (2011).
8. L. Stephens *et al.*, *Science* **365**, 897–902 (2019).
9. T. Giesecke *et al.*, *Nat. Commun.* **10**, 5422 (2019).
10. L. Marquer *et al.*, *Quat. Sci. Rev.* **171**, 20–37 (2017).
11. C. N. H. McMichael, *New Phytol.* **229**, 2492–2496 (2021).
12. C. Nolan *et al.*, *Science* **361**, 920–923 (2018).
13. D. A. Fordham *et al.*, *Science* **369**, eabc5654 (2020).
14. J. W. Williams, B. N. Shuman, T. Webb III, P. J. Bartlein, P. L. Leduc, *Ecol. Monogr.* **74**, 309–334 (2004).
15. Y. Malhi *et al.*, *Proc. Natl. Acad. Sci. U.S.A.* **113**, 838–846 (2016).
16. F. E. Mayle, D. J. Beerling, W. D. Gosling, M. B. Bush, *Phil. Trans. R. Soc. Lond. B* **359**, 499–514 (2004).
17. F. E. Mayle, M. J. Burn, M. Power, D. H. Urrego, in *Past Climate Variability in South America and Surrounding Regions*, F. Vimeux, F. Sylvestre, M. Khodri, Eds., vol. 14 of *Developments in Paleoenvironmental Research* (Springer, 2009), pp. 89–112.
18. A. W. Seddon, M. Macias-Fauria, K. J. Willis, *Holocene* **25**, 25–36 (2015).
19. S. G. A. Flantua *et al.*, *Rev. Palaeobot. Palynol.* **223**, 104–115 (2015).
20. J. W. Williams *et al.*, *Quat. Res.* **89**, 156–177 (2018).
21. O. Mottl *et al.*, bioRxiv 2020.12.16.422943 [Preprint]. 24 February 2021. https://doi.org/10.1101/2020.12.16.422943.
22. See supplementary materials online.
23. Z. Liu *et al.*, *Science* **325**, 310–314 (2009).
24. T. M. Shanahan *et al.*, *Nat. Geosci.* **8**, 140–144 (2015).
25. G. M. MacDonald, K. V. Kremenetski, D. W. Beilman, *Phil. Trans. R. Soc. B* **363**, 2283–2299 (2008).
26. H. Zhang *et al.*, *Quaternary* **2**, 26 (2019).
27. V. F. Novello *et al.*, *Earth Planet. Sci. Lett.* **524**, 115717 (2019).
28. M. H. M. Groot *et al.*, *Clim. Past* **7**, 299–316 (2011).
29. S. G. A. Flantua *et al.*, *Clim. Past* **12**, 483–523 (2016).
30. E. C. Ellis *et al.*, *Proc. Natl. Acad. Sci. U.S.A.* **110**, 7978–7985 (2013).
31. PAGES 2k Consortium, *Nat. Geosci.* **6**, 339–346 (2013).
32. K. E. Trenberth, J. T. Fasullo, T. G. Shepherd, *Nat. Clim. Chang.* **5**, 725–730 (2015).
33. R. Marchant *et al.*, *Earth Sci. Rev.* **178**, 322–378 (2018).
34. P. Ríris, M. Arroyo-Kalin, *Sci. Rep.* **9**, 6850 (2019).
35. E. D. Lorenzen *et al.*, *Nature* **479**, 359–364 (2011).
36. A. Bevan *et al.*, *Proc. Natl. Acad. Sci. U.S.A.* **114**, E10524–E10531 (2017).
37. J. E. Tierney *et al.*, *Nature* **584**, 569–573 (2020).
38. North Greenland Ice Core Project members, *Nature* **431**, 147–151 (2004).
39. E. Monnin *et al.*, *Science* **291**, 112–114 (2001).
40. O. Mottl, S. Flantua, HOPE-UIB-BIO/Global_RoC, version v1.1, Zenodo (2021); http://doi.org/10.5281/zenodo.4972077.
41. S. G. A. Flantua *et al.*, "Mottl et al. (2021, Science) Taxonomic harmonization tables for North America, Latin America, Europe, Asia, Africa," Figshare, dataset (2021); https://doi.org/10.6084/m9.figshare.13049735.

ACKNOWLEDGMENTS

We are grateful to all data contributors to the Neotoma Paleoecology Database and data stewards for the constituent databases—African Pollen Database, European Pollen Database, IndoPacific Palaeoecology Database, Latin American Pollen Database, and North American Pollen Database—for supporting open-access data. We thank H. J. B. Birks for making suggestions on the analyses and for providing advice on the Asian taxonomic harmonization. **Funding:** O.M., S.G.A.F., K.P.B., V.A.F., and A.W.R.S. acknowledge support from the European Research Council (ERC) under the European Union's Horizon 2020 research and innovation program (grant agreement no. 741413) to H. J. B. Birks. Neotoma development has been supported by the National Science Foundation (1550707, 1550805, and 1948926) and Belmont Forum (1929476). **Author contributions:** O.M., S.G.A.F., A.W.R.S., and J.W.W. co-led and designed the study. S.G.A.F., K.P.B., V.A.F., A.W.R.S., and O.M. developed the data extraction workflow, and O.M. performed the numerical analyses. J.W.W., H.H., S.G.A.F., K.P.B., and S.I. led the compilation and taxonomic harmonization of continental-scale pollen datasets. E.C.G., T.G., S.H., H.H., S.I., S.G.A.F., and J.W.W. led Neotoma data mobilization efforts. S.G.A.F. and J.W.W. led the writing. All authors contributed to the article and approved the submitted version. **Competing interests:** The authors declare no competing interests. **Data and materials availability:** All the data and R codes are publicly available at Zenodo (*40*) and at https://github.com/HOPE-UIB-BIO/Global_RoC. Harmonization tables are available at Figshare (*41*).

SUPPLEMENTARY MATERIALS

science.sciencemag.org/content/372/6544/860/suppl/DC1
Materials and Methods
Figs. S1 to S7
Tables S1 to S3
References (*42*–*77*)
Data S1

19 December 2020; accepted 8 April 2021
10.1126/science.abg1685

Global acceleration in rates of vegetation change over the past 18,000 years

Ondrej Mottl, Suzette G. A. Flantua, Kuber P. Bhatta, Vivian A. Felde, Thomas Giesecke, Simon Goring, Eric C. Grimm, Simon Haberle, Henry Hooghiemstra, Sarah Ivory, Petr Kunes, Steffen Wolters, Alistair W. R. Seddon and John W. Williams

Science **372** (6544), 860-864.
DOI: 10.1126/science.abg1685originally published online May 20, 2021

The pace of Holocene vegetation change

Although much is known about the rapid environmental changes that have occurred since the Industrial Revolution, the patterns of change over the preceding millennia have been only patchily understood. Using a global set of >1100 fossil pollen records, Mottl *et al.* explored the rates of vegetation change over the past 18,000 years (see the Perspective by Overpeck and Breshears). The authors show that the rates of change accelerated markedly during the Late Holocene (~4.6 to 2.9 thousand years ago), even more rapidly than the climate-driven vegetation changes associated with the end of the last glacial period. In addition, the Late Holocene acceleration began for terrestrial communities as a whole, suggesting that the acceleration in turnover over the past two centuries is the tip of a deeper trend.

Science, abg1685, this issue p. 860; see also abi9902, p. 786

Supplementary Materials for

Global acceleration in rates of vegetation change over the past 18,000 years

Ondřej Mottl*†, Suzette G. A. Flantua*†, Kuber P. Bhatta, Vivian A. Felde, Thomas Giesecke, Simon Goring, Eric C. Grimm, Simon Haberle, Henry Hooghiemstra, Sarah Ivory, Petr Kuneš, Steffen Wolters, Alistair W. R. Seddon, John W. Williams

*Corresponding author. Email: ondrej.mottl@gmail.com (O.M.); s.g.a.flantua@gmail.com (S.G.A.F.)
†These authors contributed equally to this work.

Published 21 May 2021, *Science* **372**, 860 (2021)
DOI: 10.1126/science.abg1685

This PDF file includes:

Other Supplementary Material for this manuscript includes the following:
(available at science.sciencemag.org/content/372/6544/860/suppl/DC1)

Data S1 (.csv)

Material and methods

Data

We obtained fossil pollen data from the Neotoma Paleoecology Database using the *neotoma* R package V1.0 (*42*) on 26th May 2020, following data mobilization campaigns by Neotoma Data Stewards for the European Pollen Database, Latin American Pollen Database, African Pollen Database, North American Pollen Database, and other Neotoma Constituent Databases. These data mobilization projects have been supported by the Human On Planet Earth (HOPE) project (Advanced ERC grant 741413 to H.J.B. Birks) (https://www.uib.no/en/rg/EECRG/107501/hope), the Abrupt Change in Climate and Ecosystems (ACCEDE) project supported by the Belmont Forum (https://www.belmontforum.org/projects/), and on-going efforts by the Neotoma Paleoecology Database (https://www.neotomadb.org), supported by the Geoinformatics and EarthCube programs at NSF.

To develop age-depth models, we selected control point types (see the included types in **Table S3**), and calibrated the radiocarbon dates using the IntCal20, SHCal20 or mixed calibration curves (*43*,*44*). Calibration curves were assigned based on the geographical location of the records and the recommended boundaries provided by *44*. For each sequence with at least five chronological control points, we constructed an age-depth model using the *bchron* R package (*45*) to generate 1000 possible age estimates for all sample depths at the original sampling resolution of the original fossil pollen sequences. We used these 1000 draws to build posterior estimates of age uncertainty. We calculated the median age estimate for each sample depth to obtain the default age used in these analyses. All ages are expressed as in calibrated years before radiocarbon present (cal yr BP, where 0 yr BP = 1950 CE) or as kiloannum BP (ka), also in calibrated years before radiocarbon present.

We performed our analyses using the following delimitation of continents: North America, South America, Europe, Africa, Asia and Oceania. The boundary between North America and Latin America was placed at the border between the US and Mexico, while the boundary between Europe and Asia was placed at the border between Russia and adjacent countries in Eastern Europe, including Finland, Belarus, Ukraine, Bulgaria, and Greece. Taxa lists for North America, Latin America, Europe, Africa, and Asia were harmonized to the taxonomically highest-precision pollen morphotypes identifiable by most palynologists. The European harmonization was adjusted from Giesecke et al. 2019 (*9*) (Level = MHVar2, http://www.europeanpollendatabase.net/data/downloads/image/EPD_P_VARS_high3.csv). Taxonomic harmonizations for other regions were developed for this paper specifically (North America) or as part of the HOPE project (Asia, Latin America) or ACCEDE project (Africa; *46*) and are available at *41*. Data from Oceania sequences were used at the original site-level taxonomic resolution. In each fossil pollen sequence, we excluded 1) all samples that contained less than 150 pollen grain counts of terrestrial taxa, 2) all samples with an age older than 18 ka, and 3) all samples for which the age has been extrapolated for more than 3000 yr. We fully excluded marine sequences, all sequences spanning less than 5000 yr, and all sequences with fewer than five samples.

Identification of sub-continental regions by cluster analysis

To study variations in rates of change in vegetation at sub-continental scales, we performed cluster analyses based on geographical and contemporary climatic features of the fossil pollen sequences (**Figs. S4, S5**). Geographical coordinates for sequences (longitude, latitude, elevation) were obtained from Neotoma, while climate variables were obtained from CHELSA (*47*) based on climate normals for 1979–2013: a) Annual Mean Temperature (BIO1; [℃*10]), b) Temperature Seasonality (BIO4; ℃, standard deviation × 1000), c) Precipitation of Driest Quarter (BIO17; [mm]), and d) Precipitation Seasonality (BIO15, [mm], coefficient of variation).

We used the *NbClust* package (*48)* to identify sub-continental regions, 'clusters', for each continent and to select an optimal number of clusters. Cluster analysis was performed separately for the six continents shown in **Fig. 2**. Clusters were created using the seven previously mentioned geographic and climatic variables (each of them standardized and centralized). We selected *McQuitty* as the clustering method and the *Manhattan distance* to calculate distances among climate and geographic variables, because they result in geographically homogeneous clusters, at a granularity appropriate for this global-scale synthesis. Note that any clustering of continuous data will be sensitive to the choice of clustering method and distance metric (*49*), so the clusters shown here should be viewed as useful data-driven tools for understanding subcontinental-scale variations in vegetation RoCs, but they are not definitive groupings. For this reason, the major findings of this paper are primarily reported at the continental scale.

The minimum and maximum number of clusters were prescribed as 3 and 10, following a similar rationale that at least three clusters were needed to assess subcontinental-scale variations, while more than 10 produced more granularity than needed for this global-scale analysis and risked clusters represented by few or outlier datasets). We accepted all subcontinental clusters for display and analysis, except for North America (**Fig. 4**), where the ten clusters originally identified led to an overly dense figure because North and South America are shown simultaneously. For North America only, we did a post-hoc combination of three of the original clusters, all in Alaska and Northwestern Canada into one cluster, to simplify the visual presentation. The original *McQuitty* clustering for North America, i.e. prior to the post-hoc combination, is available in **Fig. S7**.

Rate of Change and Peak Point estimation

We estimated the rate of change (RoC) score as well as the presence of a rapid change in taxonomic composition (i.e. 'peak points') using the R-Ratepol package (*21*, *50*). RoC analysis estimates the magnitude of compositional change per unit time, and so is a measure of community turnover that is related to, but distinct from, most beta diversity metrics, which usually focus on species presence/absence data,

and may or may not follow a standard time step. Pollen data were smoothed using an age-weighted average, in which samples were downweighted based on their temporal distance from the focus age (*51*). RoC was calculated using the chi-squared coefficient metric of dissimilarity (*52*) and between consecutive time intervals. To avoid artifactual variations in RoC caused by irregular temporal sampling resolution in the original pollen sequences (*53*), Mottl et al. (*21*) developed a new approach that employs a variant of a moving window, and is based on the following sequence: time bins of temporal width T are created, one pollen sample is selected as representative of each bin, and RoC between bins is calculated. The brackets of time bins (window) are then moved forward by a fixed time step (S), levels are selected again, and RoC calculated for a new set of time bins. This is repeated five times while retaining all the results. For the results shown in the main text, we set bin width (T) to 500 years (see section Sensitivity Analyses: Bin Width), and time increment (S) to 100 years (i.e. five window shifts). *R-Ratepol* also incorporates uncertainties in pollen sampling and uncertainties from age-depth models. In each randomization, 150 pollen grains are randomly sampled in each level and a single age sequence from age uncertainties is randomly selected. The total number of randomizations is set to 1000. For each point, the median value of all RoC scores from all randomizations is used as the final RoC score.

Peak points are defined as a significantly rapid increase in RoC score within individual sequences, and are identified using a general additive model (GAM). For each RoC sequence, a GAM is fitted using variables RoC and Age as $GAM(RoC \sim s(Age, k = 8)$. Residuals are calculated as the distance between the original point-level value and the GAM fitted value, and the standard deviation of all residuals is tracked. A RoC value is considered significantly large (i.e. a peak) if its residual is at least 2 standard deviations higher than the fitted GAM. This identification of peak points provides a standard approach for comparison among sequences and identification of time intervals characterized by increased RoCs across many sequences.

Some palynological indices of biodiversity and compositional RoC can be sensitive to variations in rare pollen taxa, which in turn are often subject to higher uncertainty due to small counts (*52, 54, 55*). To reduce

the sensitivity of these analyses to the uncertainties associated with rare types, we made two analytical decisions. First, we employed the chi-squared metric because it is in a class of signal-to-noise dissimilarity metrics that is suitable for pollen counts with rare taxa (*52*). Previous studies have tested the skill of different dissimilarity metrics when applied to fossil pollen data, e.g. for discriminating whether pollen assemblages are from the same or different vegetation types (*54*, *55*). Signal-to-noise metrics, which includes the chi-squared coefficient, have the highest skill because they draw signals from all pollen types while upweighting the more abundant types, which are less subject to counting and identification uncertainties than the rare taxa (*54*, *55*). In the context of this study, rare taxa can be expected to contribute to the RoCs but will receive less weight than more abundant taxa. Second, the random sampling method described above standardizes the pollen grains to a total of 150 pollen grains, reducing the number of rare taxa. Furthermore, we performed an additional sensitivity test for the influence of rare taxa (<1% of pollen counts) on our rate of change estimates (see below) to confirm that calculated rates of change were not sensitive to the high uncertainties associated with rare taxa.

Continental and regional RoC trends

For each continent and sub-continental cluster, we pooled sequence-level RoC values into 500-yr bins (or, for some sensitivity analyses, 250-yr bins) and calculated the 95% quantile score to focus on areas of large vegetation changes while reducing sensitivity to outliers (see section below, *Summary Statistics: Behavior and Sensitivity of the Median and 95th Quantile*). For each region, we also calculated the proportion of peak points found per interval, relative to the distribution of samples across all sequences of a selected time bin. We then constructed a GAM of the RoC values as $gam(RoC \sim s(time, k,\ bs = 'tp'))$ with a Tweedie error distribution (with a self-estimated power parameter) and weights defined as $weights = 1 + \left(\frac{the\ number\ of\ samples\ in\ time\ bin}{mean\ number\ of\ samples\ in\ all\ bins}\right)$. In order to avoid overfitting of the data while still reasonably estimating the shape of the GAM curve, we followed the routine recommended within the *mgcv* package in which a starting number of basis functions (k) was selected and the fit of the GAM to the data was checked,

using the *k.check* function from the *mgcv* package (*56*, *57*). If a sufficient fit was reached, based on randomly re-shuffled residuals (*58*), then the GAM model was complete. If not, k was increased in each step until a sufficient fit was found. The choice of *k* effectively determines the degrees of freedom in the GAM model, with higher *k* enabling a closer fit to data, while a too-high *k* will result in overfitting (*58*). In this study the starting value of k was selected as 8 and each step increased by 4. To detect the significant deviations of the GAM curve, we used the *fderiv* function from *gratia* package (*57*). Changes are considered significant if the simultaneous confidence intervals of the first derivative of the GAM function differ from zero (*56*). We followed a similar approach for the peak points, in which we constructed a GAM as $gam(PeakProportion \sim s(time, k, bs = 'tp'))$ with beta error distribution. For the cluster-level GAMs, we included only clusters with at least 10 fossil pollen sequences, to ensure that there were sufficient data points for the RoC calculations to represent regional patterns instead of patterns driven by localized signals in individual sequences.

To identify the timing of onset of the Late Holocene increases in RoC, we followed a simple algorithm in which we began at the topmost time interval and then worked backwards in time to find the first point of the continental RoC GAM curve that is significantly increasing (i.e. confidence intervals of the first derivative of the GAM curve differ from zero).

Sensitivity Analyses: Bin Width

To test the sensitivity of our analyses to choice of bin width (T), we conducted sensitivity experiments with bin widths of 500 years (**Fig. 2**) and 250 years (**Fig S2**; **Tables S1, S2**). We chose these bin widths based upon several criteria. First, 500 years is a standard resolution for mapped syntheses of late Quaternary pollen records that allows analysis of ecological responses to millennial-scale climate change during the last deglaciation while also avoiding false temporal precision given radiocarbon dating uncertainties (*59*–*61*). Second, the density of sequences and samples varies among time periods and continents and is highest

for the Holocene in Europe, eastern North America, and northwest South America (where a 250-year time bin would be best supported by data) and lower for other time periods and regions.

The first-order temporal patterns of RoCs and peak points are insensitive to choice of bin width. Regardless of choice of bin width, a Late Holocene acceleration is observed for most continents (**Figs. 2, S2**). Moreover, Late Holocene rates of compositional change remain similar to or greater than rates of change during the Pleistocene-Holocene transition. One question we aimed to address was whether the timing of the Late Holocene acceleration might be attributable to choice of bin width and the degree to which recent rapid changes in vegetation composition are smoothed backwards in time, e.g. in North America where rates of land cover conversion have been particularly rapid following Euro-American arrival (*62, 63*). However, a comparison of the data points in **Fig. 2** (500-year bin) and **Fig. S2** (250-year bin) shows remarkably little difference in timing of the late-Holocene acceleration for data-dense continents such as North America and Europe. The biggest difference is that the plotted data are noisier when the 250-year bins are employed, particularly for times and places where data densities are lower (**Fig. 1A,E**). As a result, the GAMs often fit poorly to the data binned at 250-year timesteps (**Fig. S2**). Hence, we opted to base our analyses on the data binned at 500-year timesteps, while retaining the 250-year binning for this sensitivity analysis. We do not attempt here to formally attribute the Late Holocene acceleration in North America. However, this acceleration likely is due to some combination of a growing anthropogenic footprint associated with Early to Late Woodland cultures in eastern North America (*64–69*), Late Holocene climate changes associated with declining summer insolation and unforced multi-centennial climate variability (*70*), and the dramatic transformations of North American vegetation ca. 1650 to 1850 AD associated with European arrival and intensified land use (*63*, *71*, *72*).

Sensitivity Analyses: Rare Taxa

To confirm that our results are not unduly affected by uncertainties in rare types, we ran our analyses with a percentage threshold applied to all fossil pollen spectra, in which all taxa representing less than 1% of

total pollen terrestrial shrub, herb and tree pollen counts in each sequence were removed (**Fig. S3**). We observe that the main patterns and conclusions remain consistent for all continents, though some periods of high peak points are now more exaggerated (Africa) or smoothed (Oceania, Latin America) in lower data density areas. Overall, the removal of rare taxa seems to strengthen the detection of synchronous periods of abrupt vegetation change in all continents of the Northern Hemisphere and Latin America, with slightly higher values in the proportion of peak points compared to **Figs. 2** and **S3**. However, overall trends remain similar to the results based on the all-taxa dataset. The estimated timing of the Late Holocene increase in RoC is not influenced by the inclusion of rare types (**Fig. S3**; **Table S3**). Hence, these analyses and conclusions are generally robust to the inclusion or omission of rare taxa.

Summary Statistics: Behavior and Sensitivity of the Median and 95th Quantile

We chose the 95% quantile of RoC as a summary metric because initial data explorations indicated that the mean and median were insensitive indicators of past vegetation change, particularly for the late-glacial and Early Holocene (**Fig. S6**). All continents and metrics show the Late Holocene rise in vegetation RoCs, but the median expression of vegetation RoCs is muted during earlier time intervals (**Fig. S6**), despite the large known changes in vegetation during the last deglaciation (*12*, *17*, *73–77*). For any given time period, the distribution of RoCs tends to be skewed, with many sequences showing moderate amounts of change, and some sequences showing substantial changes (**Fig. S6**). This phenomenon is well illustrated in Europe and North America, in which heightened rates of vegetation RoCs at the Pleistocene-Holocene transition at 11.7 ka are clearly visible in many individual sequences, yet the variations in the median are subtle. We attribute this apparent insensitivity of the median to the increasing effects of temporal uncertainty for earlier time periods. Because radiocarbon dates have a typical analytical uncertainty of several decades during the Late Holocene, versus several centuries at the Pleistocene-Holocene transition, there is a stronger inter-sequence blurring effect for earlier time intervals, which will be more strongly expressed in summary statistics that rely upon the median and mean. Moreover, age estimates for the Late Holocene are anchored by a date of high precision – the present – which has no counterpart across all the Lateglacial and Early Holocene

records. Hence, we view the 95% quantile as a more sensitive indicator of vegetation changes for earlier time intervals. However, for areas and times with very low sequence density, such as Oceania, the 95% quantile is likely to be overly sensitive to outlier records. Hence, interpretations in this paper focus on areas and times of higher data density.

Figures and tables

Fig. S1

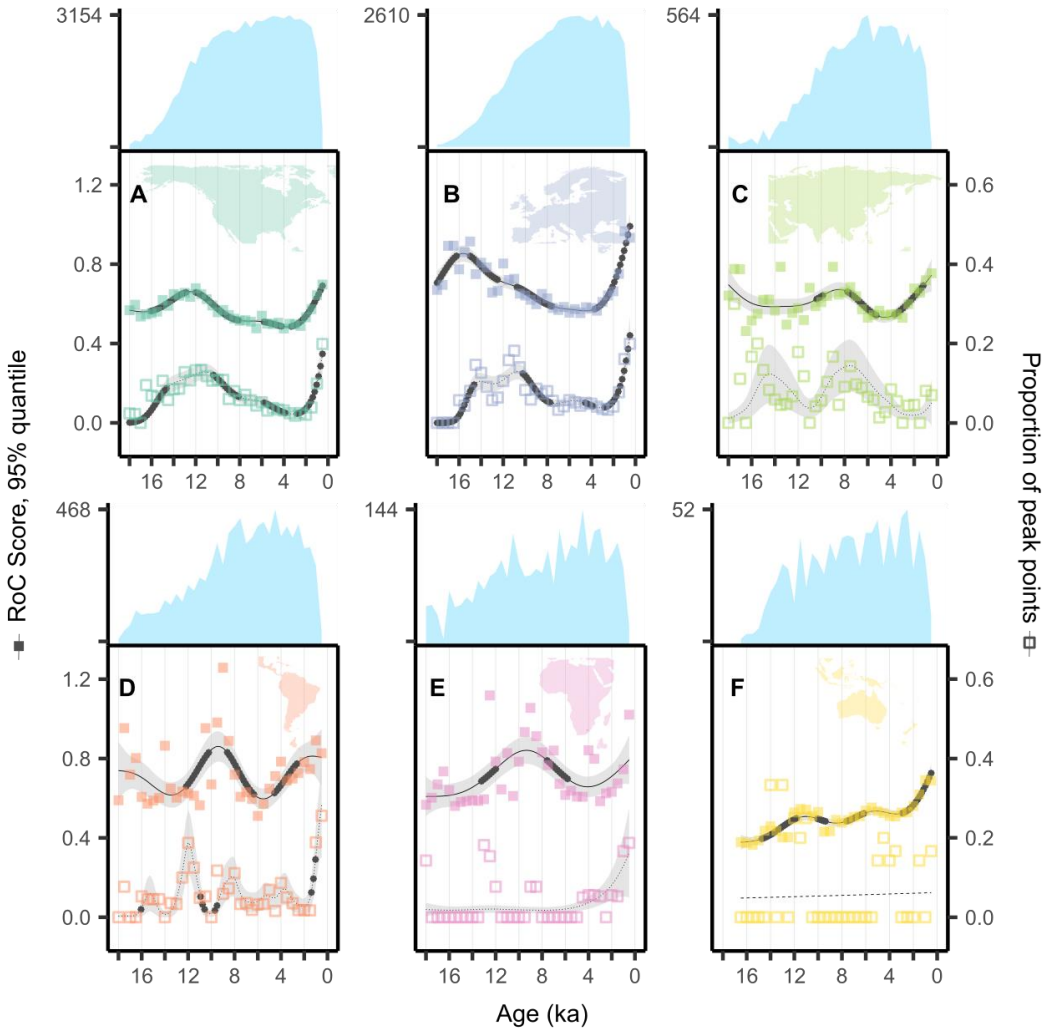

Fig. S1. Rates of Change (RoC) analyses and sample density by continent. Blue histograms indicate the number of samples per time interval. The rate-of-change and peak point squares and curves are identical to Fig. 2 and follow the same figure design. Solid line and filled squares represent the upper 95% quantile RoC score (bottom x-axis) where increased values indicate high change within the vegetation composition relative to time. The dotted line and empty squares represent the proportion of peak points within a time bin (*500 yr*) which is an indication of the degree of synchrony in RoC among sequences. When the relationship is not significant, the line is shown as dashed and the error envelope is not shown. Asterisks on the GAM curves identify where the curve significantly changes its course (i.e. where the derivative is significantly different from zero).

Fig. S2

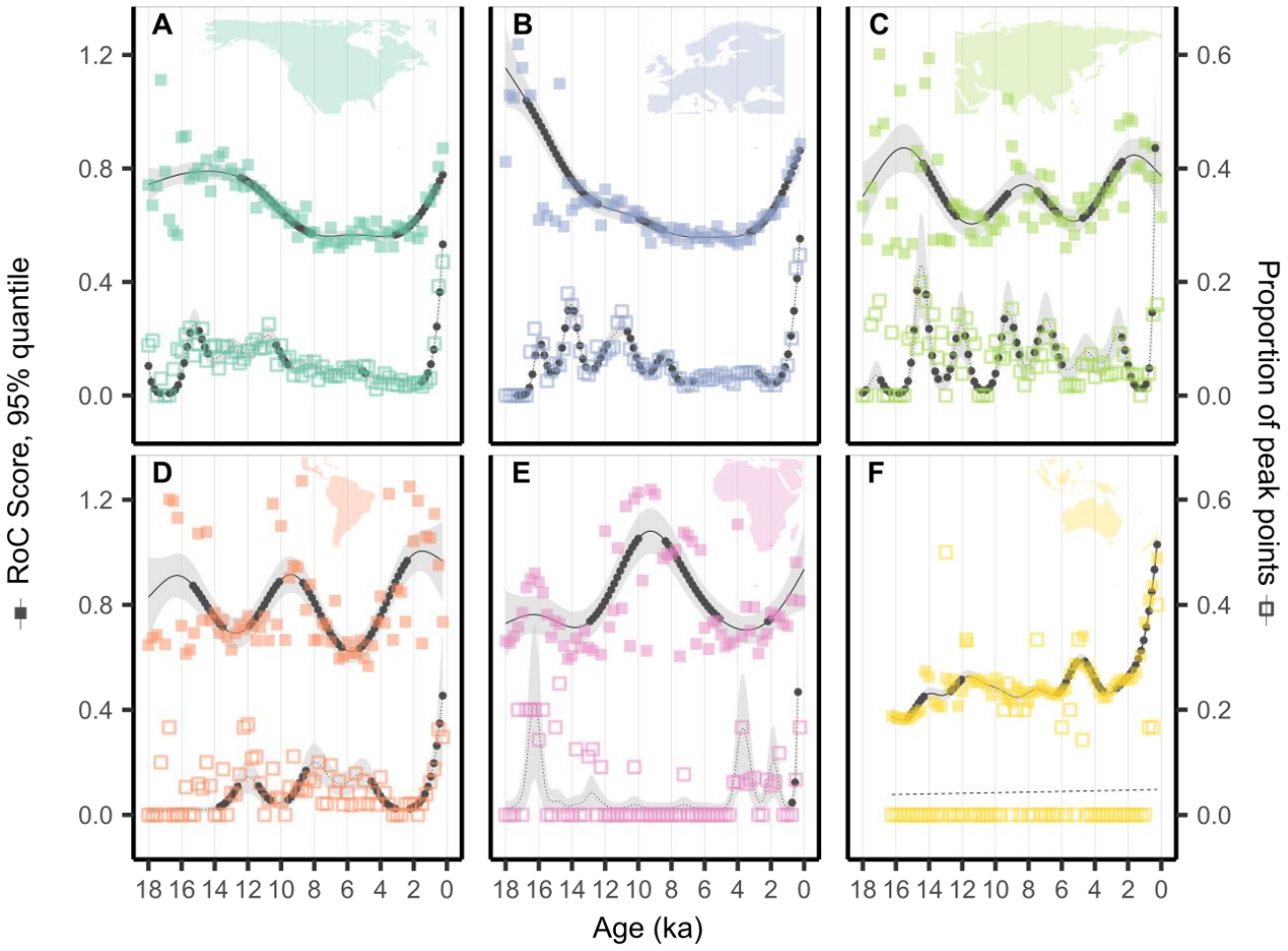

Fig. S2. Rates of Change (RoC) analyses by continent, for a sensitivity analysis with a temporal bin width of 250 years. The analyses shown here are identical to those shown in Figure 2, except that here the temporal bin width (*T*) is 250 years instead of 500 years. Figure design follows Fig. 2. See also Table S1.

Fig. S3

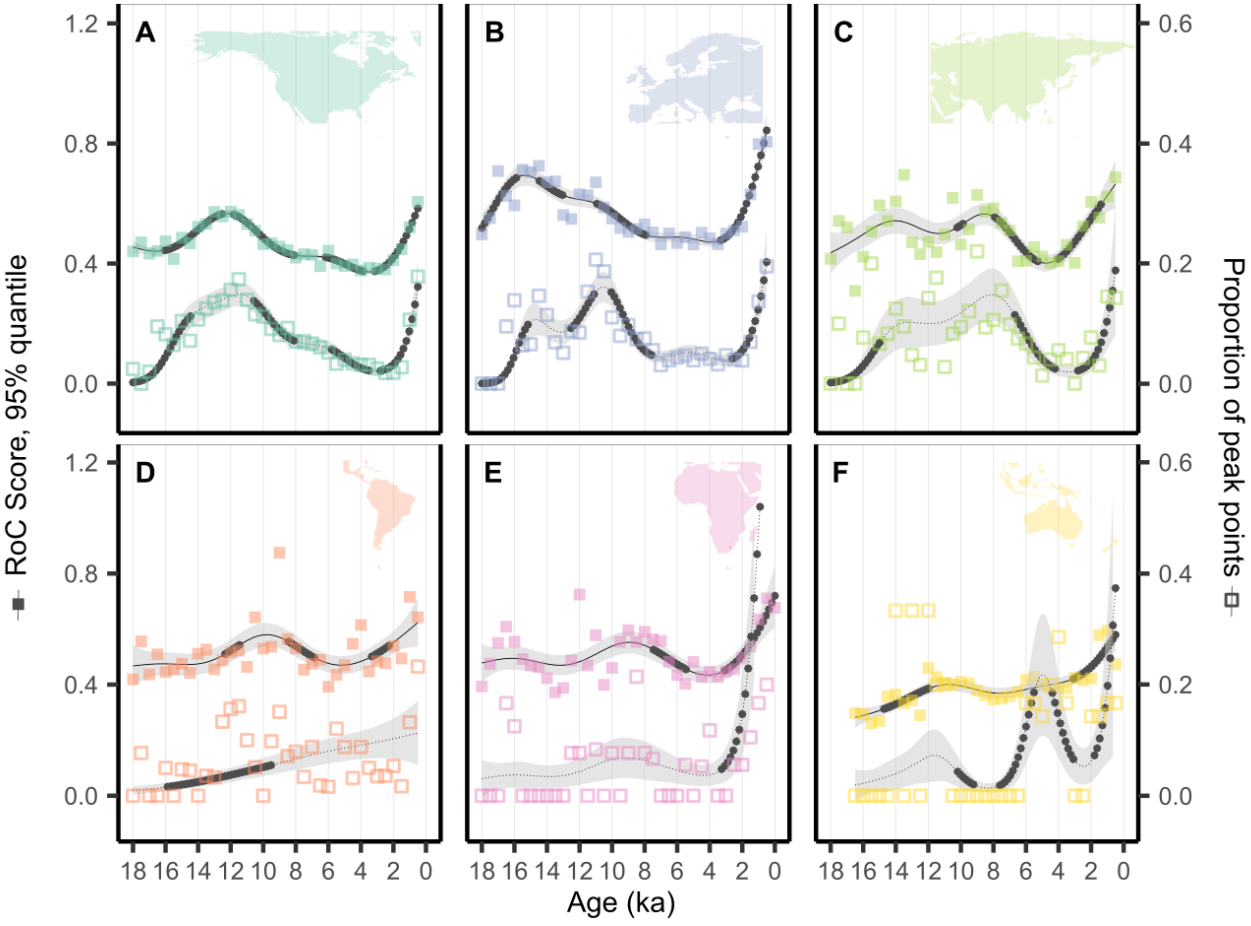

Fig. S3. Rates of Change (RoC) analyses by continent based on a sensitivity analysis that excludes rare pollen taxa. The analyses shown here are identical to those shown in Figure 2, except that all taxa representing less than 1% of total pollen counts in a given sequence were removed from that sequence. Figure design follows Fig. 2.

Fig. S4

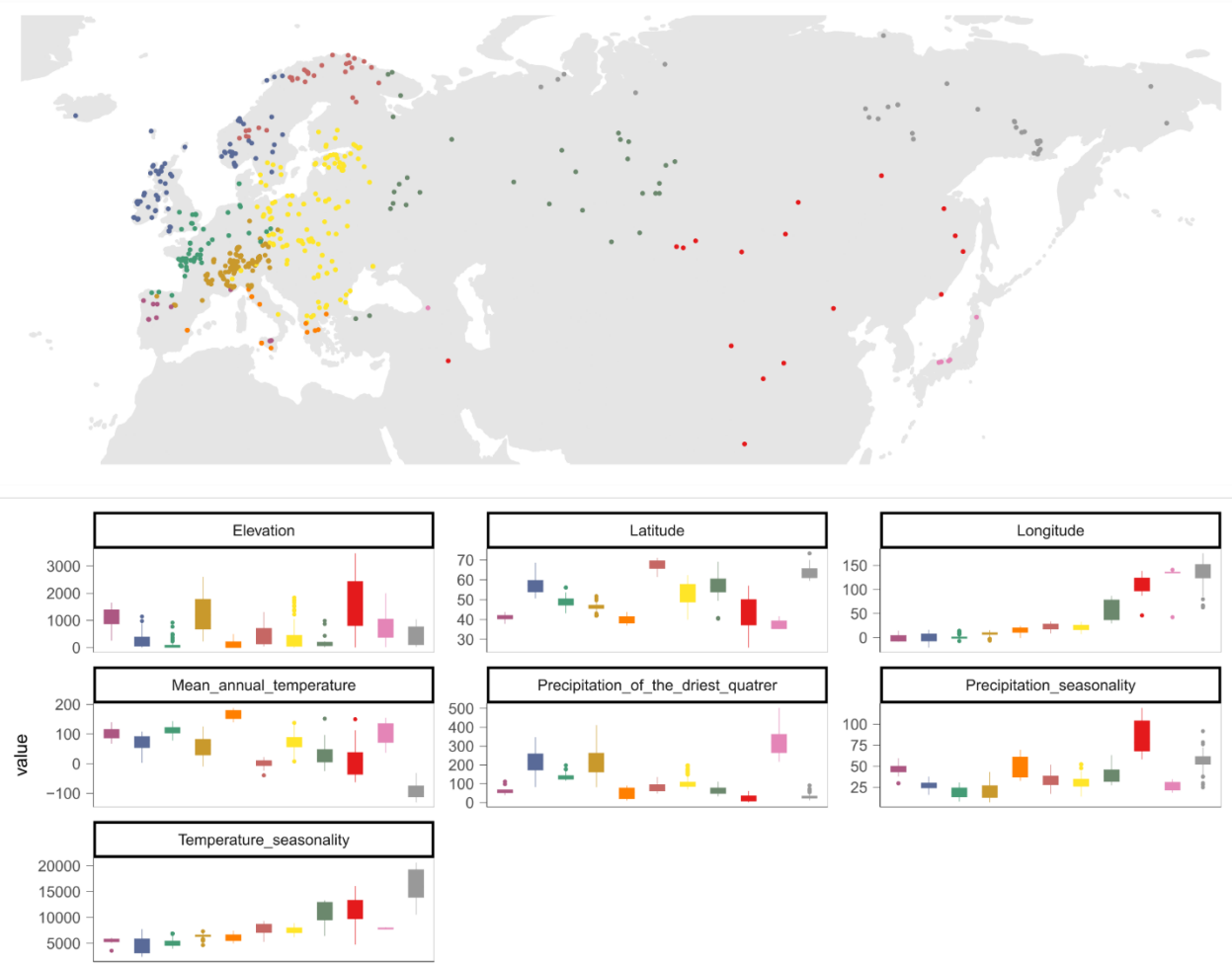

Fig. S4. Environmental characterization of identified clusters for Eurasia. Fossil pollen sequences were assigned to clusters based on geographic and environmental properties (location, elevation, climate) at present. Colors from the boxplots correspond to the colors of the clusters displayed in the map. Elevation = meters above sea level, latitude = degrees north, longitude = degrees east, mean annual temperature [°C*10], total precipitation of the driest quarter (mm/quarter), precipitation seasonality (coefficient of variation), temperature seasonality (standard deviation *1000). See section on "Identification of sub-continental regions by cluster analysis" for more information about the methods used to identify clusters.

Fig. S5

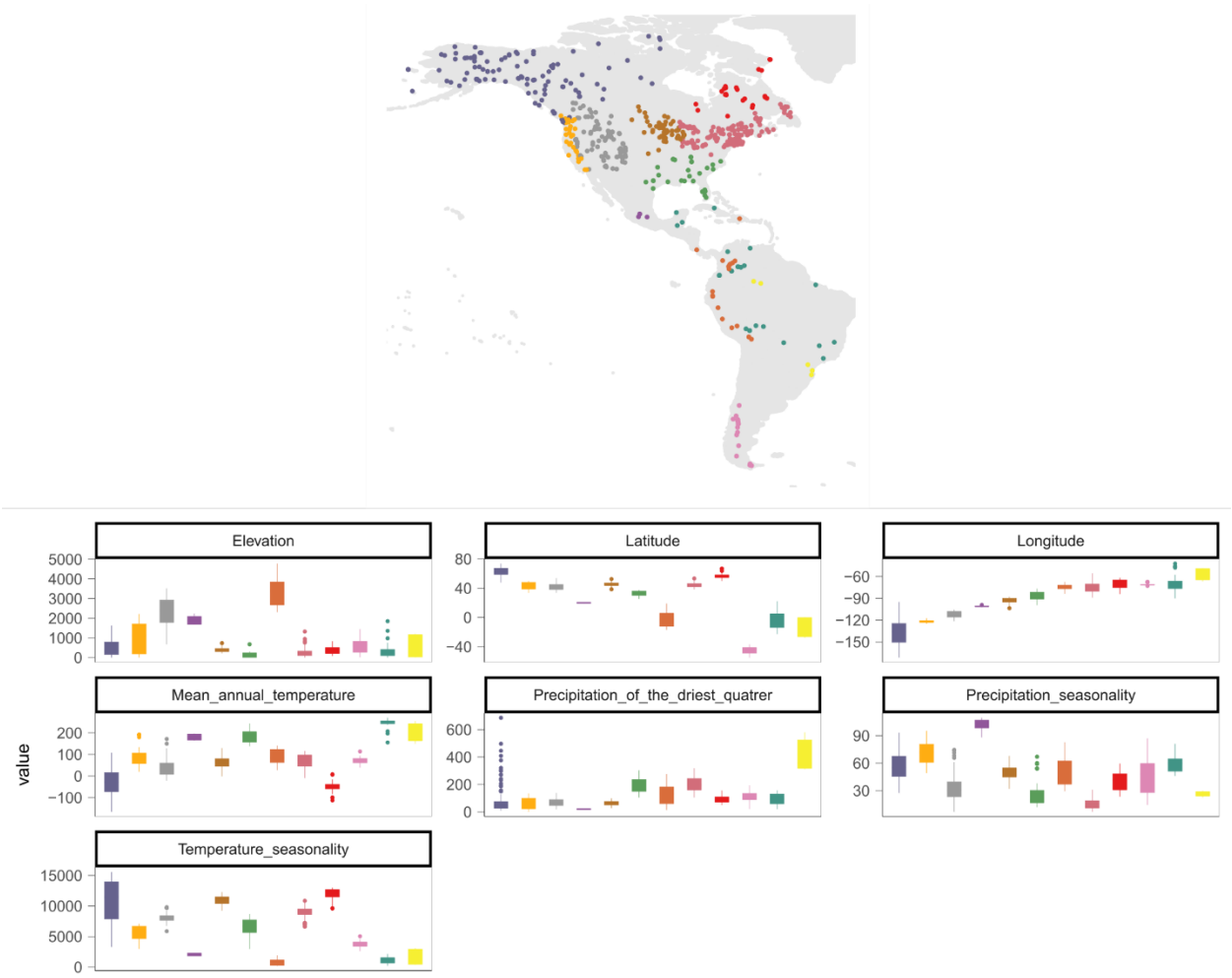

Fig. S5. Environmental variables for each cluster across the Americas. Figure design follows Fig. S4.

Fig. S6

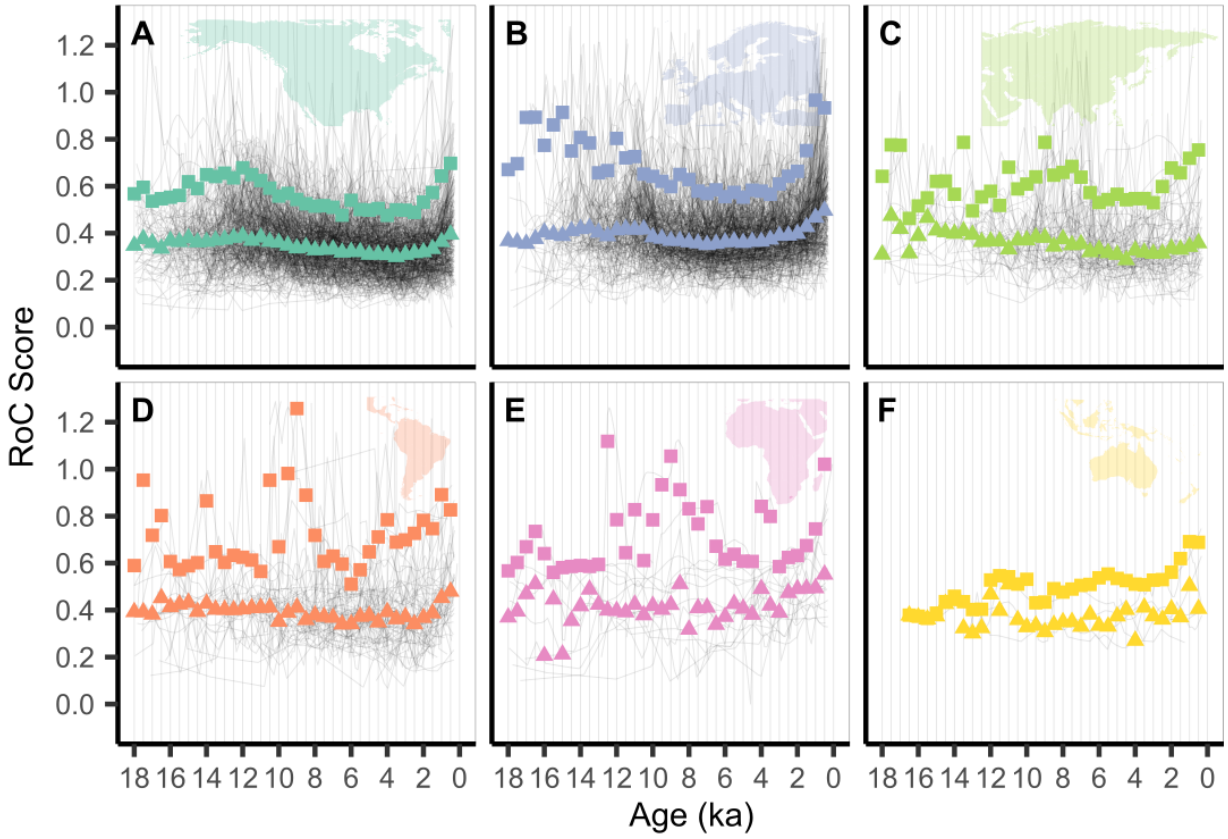

Fig. S6. Sequence-level Rates of Change (RoC) and summary statistics by continent, for both the median and 95th quantile. RoCs from individual sequences are shown as light gray lines. The 95th quantile is shown as filled squares and the median is shown as filled triangles. Color shading indicates continent, following the styles used in Figs 1, 2, and elsewhere.

Fig. S7

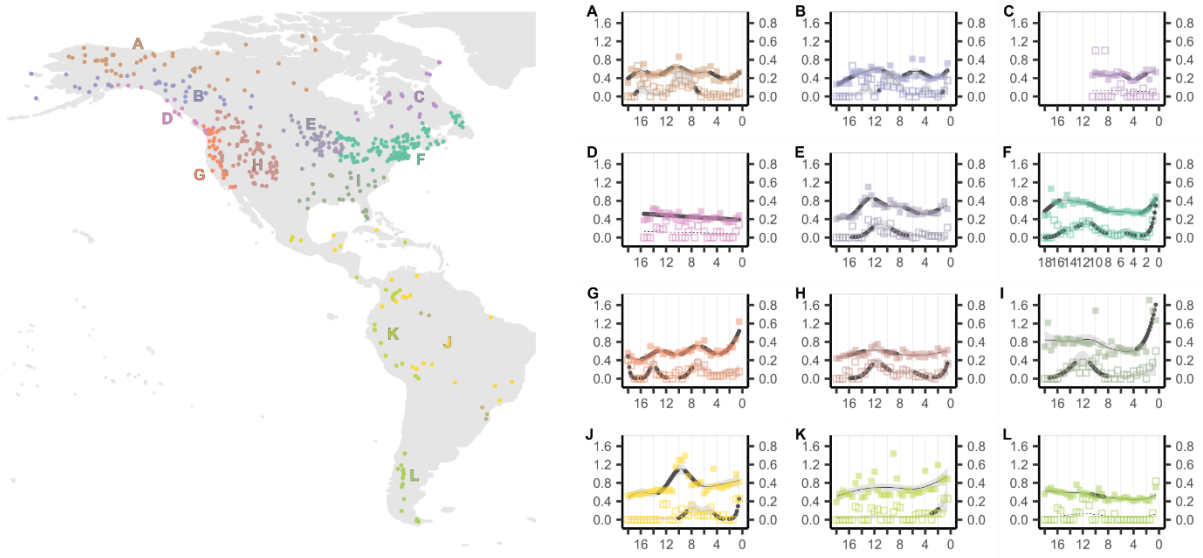

Fig. S7. All identified clusters across the Americas with their corresponding Rates of Change (RoC) analyses. This figure displays all identified clusters across the Americas according to the performed cluster analyses. For visualization purposes in Fig. 4, we merged clusters A, B, and D to one cluster A.

Table S1

Continent	Pleistocene-Holocene transition RoC maximum		Late Holocene RoC maximum		Late Holocene RoC increase (%)	Onset of Late Holocene acceleration (ka)	Explained variability of model
	Age (ka)	RoC score	Age (ka)	RoC score			
North America	12.5	0.66	0.5	0.69	4.4	3.3	0.93
Latin America	9.3	0.86	1.2	0.81	-6.2	4.6	0.43
Europe	15.7	0.85	0.5	0.99	14.1	3.7	0.89
Africa	9.3	0.84	0.5	0.79	-6.3	NA	0.37
Asia	8.5	0.67	0.5	0.75	10.7	3.7	0.47
Oceania	11	0.51	0.5	0.73	30.1	2.9	0.85

Table S1. Summary table for GAM results shown in Fig. 2. Columns 1 and 3 show the RoC scores for the two maxima (indicated by arrows in Fig. 2) identified during the last 18 ka, while column 2 shows the timing of the Lateglacial to Early Holocene maximum, and column 4 shows the timing of the Late Holocene maximum in the fitted GAM. Column 5 shows the percent increase in RoC during the Late Holocene, relative to its value at time of onset, while column 6 shows the estimated time of onset for the Late Holocene increase. The identification of the onset of the Late Holocene increase is based upon the GAM detection of statistically significant increases in rates of change, and specifically by first identifying the Late Holocene accelerations found at the end of almost all records, then identifying the first-time interval in this series with a statistically significant increase in vegetation rate of change. Column 7 shows the explained variability of the GAM models shown in Fig. 2, which is expressed as a percentage of variability of fitted model GAM. Calculations are based on 500 yr time bins. A lack of a significant increase in RoC values during the last Holocene is indicated by NA.

Table S2

No.	Region	Onset of Late Holocene acceleration (ka)	Explained variability of model
1	Fig. 3A	2.8	0.86
2	Fig. 3B	6.4	0.63
3	Fig. 3C	3.2	0.64
4	Fig. 3D	3.0	0.39
5	Fig. 3E	3.3	0.49
6	Fig. 3F	2.5	0.67
7	Fig. 3G	NA	0.47
8	Fig. 3H	4.0	0.78
9	Fig. 3I	4.6	0.64
10	Fig. 3J	NA	0.17
11	Fig. 4A	2.1	0.64
12	Fig. 4B	3.3	0.76
13	Fig. 4C	NA	0.4
14	Fig. 4D	NA	0.22
15	Fig. 4E	NA	0.55
16	Fig. 4F	3.4	0.50
17	Fig. 4G	3.3	0.75
18	Fig. 4H	3.0	0.77
19	Fig. 4I	3.5	0.51
20	Fig. 4J	NA	0.63

Table S2. Onset of the Late Holocene acceleration in rates of vegetation change among sub-continental regions. See detailed description Table S1.

Table S3

Control point type
"Annual laminations (varves)"
"Annual laminations (varves)/Sedimentation rate"
"Caesium-137"
"Collection date"
"Core top"
"Core top, estimated"
"Guess"
"Lead-210"
"Oxygen-18"
"Pb/Cs+AMS 14C"
"Radiocarbon"
"Radiocarbon, average of two or more dates"
"Radiocarbon, calibrated"
"Radiocarbon, calibrated from calendar years"
"Radiocarbon, calibrated, combined"
"Radiocarbon, infinite"
"Radiocarbon, reservoir correction"
"Radiocarbon, reservoir correction, calibrated"
"Section top"
"Tephra"

Table S3. List of accepted chronological control point types.

Data S1. (separate file)

Metadata of fossil pollen datasets used in the analyses. Dataset.id, sequence name, coordinates, elevation, REGION (continent), References, CHELSA climate variables

References and Notes

1. B. J. McGill, M. Dornelas, N. J. Gotelli, A. E. Magurran, Fifteen forms of biodiversity trend in the Anthropocene. *Trends Ecol. Evol.* **30**, 104–113 (2015). doi:10.1016/j.tree.2014.11.006 Medline

2. M. Dornelas, L. H. Antão, F. Moyes, A. E. Bates, A. E. Magurran, D. Adam, A. A. Akhmetzhanova, W. Appeltans, J. M. Arcos, H. Arnold, N. Ayyappan, G. Badihi, A. H. Baird, M. Barbosa, T. E. Barreto, C. Bässler, A. Bellgrove, J. Belmaker, L. Benedetti-Cecchi, B. J. Bett, A. D. Bjorkman, M. Błażewicz, S. A. Blowes, C. P. Bloch, T. C. Bonebrake, S. Boyd, M. Bradford, A. J. Brooks, J. H. Brown, H. Bruelheide, P. Budy, F. Carvalho, E. Castañeda-Moya, C. A. Chen, J. F. Chamblee, T. J. Chase, L. Siegwart Collier, S. K. Collinge, R. Condit, E. J. Cooper, J. H. C. Cornelissen, U. Cotano, S. Kyle Crow, G. Damasceno, C. H. Davies, R. A. Davis, F. P. Day, S. Degraer, T. S. Doherty, T. E. Dunn, G. Durigan, J. E. Duffy, D. Edelist, G. J. Edgar, R. Elahi, S. C. Elmendorf, A. Enemar, S. K. M. Ernest, R. Escribano, M. Estiarte, B. S. Evans, T.-Y. Fan, F. Turini Farah, L. Loureiro Fernandes, F. Z. Farneda, A. Fidelis, R. Fitt, A. M. Fosaa, G. A. Daher Correa Franco, G. E. Frank, W. R. Fraser, H. García, R. Cazzolla Gatti, O. Givan, E. Gorgone-Barbosa, W. A. Gould, C. Gries, G. D. Grossman, J. R. Gutierréz, S. Hale, M. E. Harmon, J. Harte, G. Haskins, D. L. Henshaw, L. Hermanutz, P. Hidalgo, P. Higuchi, A. Hoey, G. Van Hoey, A. Hofgaard, K. Holeck, R. D. Hollister, R. Holmes, M. Hoogenboom, C. H. Hsieh, S. P. Hubbell, F. Huettmann, C. L. Huffard, A. H. Hurlbert, N. Macedo Ivanauskas, D. Janík, U. Jandt, A. Jażdżewska, T. Johannessen, J. Johnstone, J. Jones, F. A. M. Jones, J. Kang, T. Kartawijaya, E. C. Keeley, D. A. Kelt, R. Kinnear, K. Klanderud, H. Knutsen, C. C. Koenig, A. R. Kortz, K. Král, L. A. Kuhnz, C.-Y. Kuo, D. J. Kushner, C. Laguionie-Marchais, L. T. Lancaster, C. Min Lee, J. S. Lefcheck, E. Lévesque, D. Lightfoot, F. Lloret, J. D. Lloyd, A. López-Baucells, M. Louzao, J. S. Madin, B. Magnússon, S. Malamud, I. Matthews, K. P. McFarland, B. McGill, D. McKnight, W. O. McLarney, J. Meador, P. L. Meserve, D. J. Metcalfe, C. F. J. Meyer, A. Michelsen, N. Milchakova, T. Moens, E. Moland, J. Moore, C. Mathias Moreira, J. Müller, G. Murphy, I. H. Myers-Smith, R. W. Myster, A. Naumov, F. Neat, J. A. Nelson, M. Paul Nelson, S. F. Newton, N. Norden, J. C. Oliver, E. M. Olsen, V. G. Onipchenko, K. Pabis, R. J. Pabst, A. Paquette, S. Pardede, D. M. Paterson, R. Pélissier, J. Peñuelas, A. Pérez-Matus, O. Pizarro, F. Pomati, E. Post, H. H. T. Prins, J. C. Priscu, P. Provoost, K. L. Prudic, E. Pulliainen, B. R. Ramesh, O. Mendivil Ramos, A. Rassweiler, J. E. Rebelo, D. C. Reed, P. B. Reich, S. M. Remillard, A. J. Richardson, J. P. Richardson, I. van Rijn, R. Rocha, V. H. Rivera-Monroy, C. Rixen, K. P. Robinson, R. Ribeiro Rodrigues, D. de Cerqueira Rossa-Feres, L. Rudstam, H. Ruhl, C. S. Ruz, E. M. Sampaio, N. Rybicki, A. Rypel, S. Sal, B. Salgado, F. A. M. Santos, A. P. Savassi-Coutinho, S. Scanga, J. Schmidt, R. Schooley, F. Setiawan, K.-T. Shao, G. R. Shaver, S. Sherman, T. W. Sherry, J. Siciński, C. Sievers, A. C. da Silva, F. Rodrigues da Silva, F. L. Silveira, J. Slingsby, T. Smart, S. J. Snell, N. A. Soudzilovskaia, G. B. G. Souza, F. Maluf Souza, V. Castro Souza, C. D. Stallings, R. Stanforth, E. H. Stanley, J. Mauro Sterza, M. Stevens, R. Stuart-Smith, Y. Rondon Suarez, S. Supp, J. Yoshio Tamashiro, S. Tarigan, G. P. Thiede, S. Thorn, A. Tolvanen, M. Teresa Zugliani Toniato, Ø. Totland, R. R. Twilley, G. Vaitkus, N. Valdivia, M. I. Vallejo, T. J. Valone, C. Van Colen, J. Vanaverbeke, F. Venturoli, H. M. Verheye, M. Vianna, R. P. Vieira, T. Vrška, C. Quang Vu, L. Van Vu, R. B. Waide, C. Waldock, D. Watts, S. Webb, T. Wesołowski, E. P. White, C. E. Widdicombe, D. Wilgers, R. Williams, S. B. Williams, M. Williamson, M. R. Willig,

T. J. Willis, S. Wipf, K. D. Woods, E. J. Woehler, K. Zawada, M. L. Zettler, T. Hickler, BioTIME: A database of biodiversity time series for the Anthropocene. *Glob. Ecol. Biogeogr.* **27**, 760–786 (2018). doi:10.1111/geb.12729 Medline

3. J. Woodbridge, R. Fyfe, D. Smith, R. Pelling, A. de Vareilles, R. Batchelor, A. Bevan, A. L. Davies, What drives biodiversity patterns? Using long-term multidisciplinary data to discern centennial-scale change. *J. Ecol.* **109**, 1396–1410 (2021). doi:10.1111/1365-2745.13565

4. E. C. Ellis, N. Ramankutty, Putting people in the map: Anthropogenic biomes of the world. *Front. Ecol. Environ.* **6**, 439–447 (2008). doi:10.1890/070062

5. S. L. Pimm, C. N. Jenkins, R. Abell, T. M. Brooks, J. L. Gittleman, L. N. Joppa, P. H. Raven, C. M. Roberts, J. O. Sexton, The biodiversity of species and their rates of extinction, distribution, and protection. *Science* **344**, 1246752 (2014). doi:10.1126/science.1246752 Medline

6. S. A. Blowes, S. R. Supp, L. H. Antão, A. Bates, H. Bruelheide, J. M. Chase, F. Moyes, A. Magurran, B. McGill, I. H. Myers-Smith, M. Winter, A. D. Bjorkman, D. E. Bowler, J. E. K. Byrnes, A. Gonzalez, J. Hines, F. Isbell, H. P. Jones, L. M. Navarro, P. L. Thompson, M. Vellend, C. Waldock, M. Dornelas, The geography of biodiversity change in marine and terrestrial assemblages. *Science* **366**, 339–345 (2019). doi:10.1126/science.aaw1620 Medline

7. D. M. J. S. Bowman, J. Balch, P. Artaxo, W. J. Bond, M. A. Cochrane, C. M. D'Antonio, R. Defries, F. H. Johnston, J. E. Keeley, M. A. Krawchuk, C. A. Kull, M. Mack, M. A. Moritz, S. Pyne, C. I. Roos, A. C. Scott, N. S. Sodhi, T. W. Swetnam, R. Whittaker, The human dimension of fire regimes on Earth. *J. Biogeogr.* **38**, 2223–2236 (2011). doi:10.1111/j.1365-2699.2011.02595.x Medline

8. L. Stephens, D. Fuller, N. Boivin, T. Rick, N. Gauthier, A. Kay, B. Marwick, C. G. Armstrong, C. M. Barton, T. Denham, K. Douglass, J. Driver, L. Janz, P. Roberts, J. D. Rogers, H. Thakar, M. Altaweel, A. L. Johnson, M. M. Sampietro Vattuone, M. Aldenderfer, S. Archila, G. Artioli, M. T. Bale, T. Beach, F. Borrell, T. Braje, P. I. Buckland, N. G. Jiménez Cano, J. M. Capriles, A. Diez Castillo, Ç. Çilingiroğlu, M. Negus Cleary, J. Conolly, P. R. Coutros, R. A. Covey, M. Cremaschi, A. Crowther, L. Der, S. di Lernia, J. F. Doershuk, W. E. Doolittle, K. J. Edwards, J. M. Erlandson, D. Evans, A. Fairbairn, P. Faulkner, G. Feinman, R. Fernandes, S. M. Fitzpatrick, R. Fyfe, E. Garcea, S. Goldstein, R. C. Goodman, J. Dalpoim Guedes, J. Herrmann, P. Hiscock, P. Hommel, K. A. Horsburgh, C. Hritz, J. W. Ives, A. Junno, J. G. Kahn, B. Kaufman, C. Kearns, T. R. Kidder, F. Lanoë, D. Lawrence, G.-A. Lee, M. J. Levin, H. B. Lindskoug, J. A. López-Sáez, S. Macrae, R. Marchant, J. M. Marston, S. McClure, M. D. McCoy, A. V. Miller, M. Morrison, G. Motuzaite Matuzeviciute, J. Müller, A. Nayak, S. Noerwidi, T. M. Peres, C. E. Peterson, L. Proctor, A. R. Randall, S. Renette, G. Robbins Schug, K. Ryzewski, R. Saini, V. Scheinsohn, P. Schmidt, P. Sebillaud, O. Seitsonen, I. A. Simpson, A. Sołtysiak, R. J. Speakman, R. N. Spengler, M. L. Steffen, M. J. Storozum, K. M. Strickland, J. Thompson, T. L. Thurston, S. Ulm, M. C. Ustunkaya, M. H. Welker, C. West, P. R. Williams, D. K. Wright, N. Wright, M. Zahir, A. Zerboni, E. Beaudoin, S. Munevar Garcia, J. Powell, A. Thornton, J. O. Kaplan, M.-J. Gaillard, K. Klein Goldewijk, E. Ellis, Archaeological assessment reveals Earth's early transformation through land use. *Science* **365**, 897–902 (2019). doi:10.1126/science.aax1192 Medline

9. T. Giesecke, S. Wolters, J. F. N. van Leeuwen, P. W. O. van der Knaap, M. Leydet, S. Brewer, Postglacial change of the floristic diversity gradient in Europe. *Nat. Commun.* **10**, 5422 (2019). doi:10.1038/s41467-019-13233-y Medline

10. L. Marquer, M.-J. Gaillard, S. Sugita, A. Poska, A.-K. Trondman, F. Mazier, A. B. Nielsen, R. M. Fyfe, A. M. Jönsson, B. Smith, J. O. Kaplan, T. Alenius, H. J. B. Birks, A. E. Bjune, J. Christiansen, J. Dodson, K. J. Edwards, T. Giesecke, U. Herzschuh, M. Kangur, T. Koff, M. Latałowa, J. Lechterbeck, J. Olofsson, H. Seppä, Quantifying the effects of land use and climate on Holocene vegetation in Europe. *Quat. Sci. Rev.* **171**, 20–37 (2017). doi:10.1016/j.quascirev.2017.07.001

11. C. N. H. McMichael, Ecological legacies of past human activities in Amazonian forests. *New Phytol.* **229**, 2492–2496 (2021). doi:10.1111/nph.16888 Medline

12. C. Nolan, J. T. Overpeck, J. R. M. Allen, P. M. Anderson, J. L. Betancourt, H. A. Binney, S. Brewer, M. B. Bush, B. M. Chase, R. Cheddadi, M. Djamali, J. Dodson, M. E. Edwards, W. D. Gosling, S. Haberle, S. C. Hotchkiss, B. Huntley, S. J. Ivory, A. P. Kershaw, S.-H. Kim, C. Latorre, M. Leydet, A.-M. Lézine, K.-B. Liu, Y. Liu, A. V. Lozhkin, M. S. McGlone, R. A. Marchant, A. Momohara, P. I. Moreno, S. Müller, B. L. Otto-Bliesner, C. Shen, J. Stevenson, H. Takahara, P. E. Tarasov, J. Tipton, A. Vincens, C. Weng, Q. Xu, Z. Zheng, S. T. Jackson, Past and future global transformation of terrestrial ecosystems under climate change. *Science* **361**, 920–923 (2018). doi:10.1126/science.aan5360 Medline

13. D. A. Fordham, S. T. Jackson, S. C. Brown, B. Huntley, B. W. Brook, D. Dahl-Jensen, M. T. P. Gilbert, B. L. Otto-Bliesner, A. Svensson, S. Theodoridis, J. M. Wilmshurst, J. C. Buettel, E. Canteri, M. McDowell, L. Orlando, J. Pilowsky, C. Rahbek, D. Nogues-Bravo, Using paleo-archives to safeguard biodiversity under climate change. *Science* **369**, eabc5654 (2020). doi:10.1126/science.abc5654 Medline

14. J. W. Williams, B. N. Shuman, T. Webb III, P. J. Bartlein, P. L. Leduc, Late-Quaternary vegetation dynamics in North America: Scaling from taxa to biomes. *Ecol. Monogr.* **74**, 309–334 (2004). doi:10.1890/02-4045

15. Y. Malhi, C. E. Doughty, M. Galetti, F. A. Smith, J.-C. Svenning, J. W. Terborgh, Megafauna and ecosystem function from the Pleistocene to the Anthropocene. *Proc. Natl. Acad. Sci. U.S.A.* **113**, 838–846 (2016). doi:10.1073/pnas.1502540113 Medline

16. F. E. Mayle, D. J. Beerling, W. D. Gosling, M. B. Bush, Responses of Amazonian ecosystems to climatic and atmospheric carbon dioxide changes since the last glacial maximum. *Phil. Trans. R. Soc. Lond. B* **359**, 499–514 (2004). doi:10.1098/rstb.2003.1434 Medline

17. F. E. Mayle, M. J. Burn, M. Power, D. H. Urrego, in *Past Climate Variability in South America and Surrounding Regions*, F. Vimeux, F. Sylvestre, M. Khodri, Eds., vol. 14 of *Developments in Paleoenvironmental Research* (Springer, 2009), pp. 89–112.

18. A. W. Seddon, M. Macias-Fauria, K. J. Willis, Climate and abrupt vegetation change in Northern Europe since the last deglaciation. *Holocene* **25**, 25–36 (2015). doi:10.1177/0959683614556383

19. S. G. A. Flantua, H. Hooghiemstra, E. C. Grimm, H. Behling, M. B. Bush, C. González-Arango, W. D. Gosling, M.-P. Ledru, S. Lozano-García, A. Maldonado, A. R. Prieto, V. Rull, J. H. Van Boxel, Updated site compilation of the Latin American Pollen Database. *Rev. Palaeobot. Palynol.* **223**, 104–115 (2015). doi:10.1016/j.revpalbo.2015.09.008

20. J. W. Williams, E. C. Grimm, J. L. Blois, D. F. Charles, E. B. Davis, S. J. Goring, R. W. Graham, A. J. Smith, M. Anderson, J. Arroyo-Cabrales, A. C. Ashworth, J. L. Betancourt, B. W. Bills, R. K. Booth, P. I. Buckland, B. B. Curry, T. Giesecke, S. T. Jackson, C. Latorre, J. Nichols, T. Purdum, R. E. Roth, M. Stryker, H. Takahara, The Neotoma Paleoecology Database, a multiproxy, international, community-curated data resource. *Quat. Res.* **89**, 156–177 (2018). doi:10.1017/qua.2017.105

21. O. Mottl, J.-A. Grytnes, A. W. R. Seddon, M. J. Steinbauer, K. P. Bhatta, V. A. Felde, S. G. A. Flantua, H. J. B. Birks, Rate-of-change analysis in palaeoecology revisited: A new approach. bioRxiv 2020.12.16.422943 [Preprint]. 24 February 2021. https://doi.org/10.1101/2020.12.16.422943.

22. See supplementary materials online.

23. Z. Liu, B. L. Otto-Bliesner, F. He, E. C. Brady, R. Tomas, P. U. Clark, A. E. Carlson, J. Lynch-Stieglitz, W. Curry, E. Brook, D. Erickson, R. Jacob, J. Kutzbach, J. Cheng, Transient simulation of last deglaciation with a new mechanism for Bolling-Allerod warming. *Science* **325**, 310–314 (2009). doi:10.1126/science.1171041 Medline

24. T. M. Shanahan, N. P. McKay, K. A. Hughen, J. T. Overpeck, B. Otto-Bliesner, C. W. Heil, J. King, C. A. Scholz, J. Peck, The time-transgressive termination of the African Humid Period. *Nat. Geosci.* **8**, 140–144 (2015). doi:10.1038/ngeo2329

25. G. M. MacDonald, K. V. Kremenetski, D. W. Beilman, Climate change and the northern Russian treeline zone. *Phil. Trans. R. Soc. B* **363**, 2283–2299 (2008). doi:10.1098/rstb.2007.2200

26. H. Zhang, Brahim, Li, Zhao, Kathayat, Tian, Baker, Wang, Zhang, Ning, Edwards, Cheng, The Asian summer monsoon: Teleconnections and forcing mechanisms—A review from Chinese speleothem δ18O records. *Quaternary* **2**, 26 (2019). doi:10.3390/quat2030026

27. V. F. Novello, F. W. Cruz, M. M. McGlue, C. I. Wong, B. M. Ward, M. Vuille, R. A. Santos, P. Jaqueto, L. C. R. Pessenda, T. Atorre, L. M. A. L. Ribeiro, I. Karmann, E. S. Barreto, H. Cheng, R. L. Edwards, M. S. Paula, D. Scholz, Vegetation and environmental changes in tropical South America from the last glacial to the Holocene documented by multiple cave sediment proxies. *Earth Planet. Sci. Lett.* **524**, 115717 (2019). doi:10.1016/j.epsl.2019.115717

28. M. H. M. Groot, R. G. Bogotá, L. J. Lourens, H. Hooghiemstra, M. Vriend, J. C. Berrio, E. Tuenter, J. Van der Plicht, B. Van Geel, M. Ziegler, S. L. Weber, A. Betancourt, L. Contreras, S. Gaviria, C. Giraldo, N. González, J. H. F. Jansen, M. Konert, D. Ortega, O. Rangel, G. Sarmiento, J. Vandenberghe, T. Van der Hammen, M. Van der Linden, W. Westerhoff, Ultra-high resolution pollen record from the northern Andes reveals rapid shifts in montane climates within the last two glacial cycles. *Clim. Past* **7**, 299–316 (2011). doi:10.5194/cp-7-299-2011

29. S. G. A. Flantua, H. Hooghiemstra, M. Vuille, H. Behling, J. F. Carson, W. D. Gosling, I. Hoyos, M. P. Ledru, E. Montoya, F. Mayle, A. Maldonado, V. Rull, M. S. Tonello, B. S. Whitney, C. González-Arango, Climate variability and human impact in South America during the last 2000 years: Synthesis and perspectives from pollen records. *Clim. Past* **12**, 483–523 (2016). doi:10.5194/cp-12-483-2016

30. E. C. Ellis, J. O. Kaplan, D. Q. Fuller, S. Vavrus, K. K. Goldewijk, P. H. Verburg, Used planet: A global history. *Proc. Natl. Acad. Sci. U.S.A.* **110**, 7978–7985 (2013). doi:10.1073/pnas.1217241110 Medline

31. PAGES 2k Consortium, Continental-scale temperature variability during the past two millennia. *Nat. Geosci.* **6**, 339–346 (2013). doi:10.1038/ngeo1797

32. K. E. Trenberth, J. T. Fasullo, T. G. Shepherd, Attribution of climate extreme events. *Nat. Clim. Chang.* **5**, 725–730 (2015). doi:10.1038/nclimate2657

33. R. Marchant, S. Richer, O. Boles, C. Capitani, C. J. Courtney-Mustaphi, P. Lane, M. E. Prendergast, D. Stump, G. De Cort, J. O. Kaplan, L. Phelps, A. Kay, D. Olago, N. Petek, P. J. Platts, P. Punwong, M. Widgren, S. Wynne-Jones, C. Ferro-Vázquez, J. Benard, N. Boivin, A. Crowther, A. Cuní-Sanchez, N. J. Deere, A. Ekblom, J. Farmer, J. Finch, D. Fuller, M.-J. Gaillard-Lemdahl, L. Gillson, E. Githumbi, T. Kabora, R. Kariuki, R. Kinyanjui, E. Kyazike, C. Lang, J. Lejju, K. D. Morrison, V. Muiruri, C. Mumbi, R. Muthoni, A. Muzuka, E. Ndiema, C. Kabonyi Nzabandora, I. Onjala, A. P. Schrijver, S. Rucina, A. Shoemaker, S. Thornton-Barnett, G. van der Plas, E. E. Watson, D. Williamson, D. Wright, Drivers and trajectories of land cover change in East Africa: Human and environmental interactions from 6000 years ago to present. *Earth Sci. Rev.* **178**, 322–378 (2018). doi:10.1016/j.earscirev.2017.12.010

34. P. Riris, M. Arroyo-Kalin, Widespread population decline in South America correlates with mid-Holocene climate change. *Sci. Rep.* **9**, 6850 (2019). doi:10.1038/s41598-019-43086-w Medline

35. E. D. Lorenzen, D. Nogués-Bravo, L. Orlando, J. Weinstock, J. Binladen, K. A. Marske, A. Ugan, M. K. Borregaard, M. T. P. Gilbert, R. Nielsen, S. Y. W. Ho, T. Goebel, K. E. Graf, D. Byers, J. T. Stenderup, M. Rasmussen, P. F. Campos, J. A. Leonard, K.-P. Koepfli, D. Froese, G. Zazula, T. W. Stafford Jr., K. Aaris-Sørensen, P. Batra, A. M. Haywood, J. S. Singarayer, P. J. Valdes, G. Boeskorov, J. A. Burns, S. P. Davydov, J. Haile, D. L. Jenkins, P. Kosintsev, T. Kuznetsova, X. Lai, L. D. Martin, H. G. McDonald, D. Mol, M. Meldgaard, K. Munch, E. Stephan, M. Sablin, R. S. Sommer, T. Sipko, E. Scott, M. A. Suchard, A. Tikhonov, R. Willerslev, R. K. Wayne, A. Cooper, M. Hofreiter, A. Sher, B. Shapiro, C. Rahbek, E. Willerslev, Species-specific responses of Late Quaternary megafauna to climate and humans. *Nature* **479**, 359–364 (2011). doi:10.1038/nature10574 Medline

36. A. Bevan, S. Colledge, D. Fuller, R. Fyfe, S. Shennan, C. Stevens, Holocene fluctuations in human population demonstrate repeated links to food production and climate. *Proc. Natl. Acad. Sci. U.S.A.* **114**, E10524–E10531 (2017). doi:10.1073/pnas.1709190114 Medline

37. J. E. Tierney, J. Zhu, J. King, S. B. Malevich, G. J. Hakim, C. J. Poulsen, Glacial cooling and climate sensitivity revisited. *Nature* **584**, 569–573 (2020). doi:10.1038/s41586-020-2617-x Medline

38. North Greenland Ice Core Project members, High-resolution record of Northern Hemisphere climate extending into the last interglacial period. *Nature* **431**, 147–151 (2004). doi:10.1038/nature02805 Medline

39. E. Monnin, A. Indermühle, A. Dällenbach, J. Flückiger, B. Stauffer, T. F. Stocker, D. Raynaud, J. M. Barnola, Atmospheric CO_2 concentrations over the last glacial termination. *Science* **291**, 112–114 (2001). doi:10.1126/science.291.5501.112 Medline

40. O. Mottl, S. Flantua, HOPE-UIB-BIO/Global_RoC: First public release, version v1.0, Zenodo (2021); http://doi.org/10.5281/zenodo.4650239.

41. S. G. A. Flantua, O. Mottl, K. P. Bhatta, V. A. Felde, T. Giesecke, S. Goring, E. C. Grimm, S. G. Haberle, H. Hooghiemstra, S. Ivory, P. Kuneš, A. W. R. Seddon, J.

Williams, “Mottl et al. (2021, Science) Taxonomic harmonization tables for North America, Latin America, Europe, Asia, Africa,” Figshare, dataset (2021); https://doi.org/10.6084/m9.figshare.13049735.

42. S. Goring, A. Dawson, G. L. Simpson, K. Ram, R. W. Graham, E. C. Grimm, J. W. Williams, neotoma: A programmatic interface to the Neotoma paleoecological database. *Open Quat.* **1**, 2 (2015). doi:10.5334/oq.ab

43. P. J. Reimer, W. E. N. Austin, E. Bard, A. Bayliss, P. G. Blackwell, C. Bronk Ramsey, M. Butzin, H. Cheng, R. L. Edwards, M. Friedrich, P. M. Grootes, T. P. Guilderson, I. Hajdas, T. J. Heaton, A. G. Hogg, K. A. Hughen, B. Kromer, S. W. Manning, R. Muscheler, J. G. Palmer, C. Pearson, J. van der Plicht, R. W. Reimer, D. A. Richards, E. M. Scott, J. R. Southon, C. S. M. Turney, L. Wacker, F. Adolphi, U. Büntgen, M. Capano, S. M. Fahrni, A. Fogtmann-Schulz, R. Friedrich, P. Köhler, S. Kudsk, F. Miyake, J. Olsen, F. Reinig, M. Sakamoto, A. Sookdeo, S. Talamo, The IntCal20 northern hemisphere radiocarbon age calibration curve (0–55 cal kBP). *Radiocarbon* **62**, 725–757 (2020). doi:10.1017/RDC.2020.41

44. A. G. Hogg, T. J. Heaton, Q. Hua, J. G. Palmer, C. S. M. Turney, J. Southon, A. Bayliss, P. G. Blackwell, G. Boswijk, C. Bronk Ramsey, C. Pearson, F. Petchey, P. Reimer, R. Reimer, L. Wacker, SHCal20 southern hemisphere calibration, 0–55,000 years cal BP. *Radiocarbon* **62**, 759–778 (2020). doi:10.1017/RDC.2020.59

45. J. Haslett, A. Parnell, A simple monotone process with application to radiocarbon-dated depth chronologies. *J. R. Stat. Soc. Ser. C Appl. Stat.* **57**, 399–418 (2008). doi:10.1111/j.1467-9876.2008.00623.x

46. A. Vincens, A.-M. Lézine, G. Buchet, D. Lewden, A. Le Thomas, African pollen database inventory of tree and shrub pollen types. *Rev. Palaeobot. Palynol.* **145**, 135–141 (2007). doi:10.1016/j.revpalbo.2006.09.004

47. D. N. Karger, O. Conrad, J. Böhner, T. Kawohl, H. Kreft, R. W. Soria-Auza, N. E. Zimmermann, H. P. Linder, M. Kessler, Climatologies at high resolution for the earth’s land surface areas. *Sci. Data* **4**, 170122 (2017). doi:10.1038/sdata.2017.122 Medline

48. M. Charrad, N. Ghazzali, V. Boiteau, A. Niknafs, NbClust: An R package for determining the relevant number of clusters in a data set. *J. Stat. Softw.* **61**, 1–36 (2014). doi:10.18637/jss.v061.i06

49. A. S. Shirkhorshidi, S. Aghabozorgi, T. Y. Wah, A comparison study on similarity and dissimilarity measures in clustering continuous data. *PLOS ONE* **10**, e0144059 (2015). doi:10.1371/journal.pone.0144059 Medline

50. O. Mottl, J.-A. Grytnes, A. W. R. Seddon, M. J. Steinbauer, K. P. Bhatta, V. A. Felde, S. G. A. Flantua, H. J. B. Birks, R-Ratepol package, Github (2020); https://github.com/HOPE-UIB-BIO/R-Ratepol-package.

51. L. Wilkinson, *The Grammar of Graphics* (Springer, ed. 2, 2005).

52. I. C. Prentice, Multidimensional scaling as a research tool in quaternary palynology: A review of theory and methods. *Rev. Palaeobot. Palynol.* **31**, 71–104 (1980). doi:10.1016/0034-6667(80)90023-8

53. A. F. Lotter, B. Ammann, M. Sturm, Rates of change and chronological problems during the late-glacial period. *Clim. Dyn.* **6**, 233–239 (1992). doi:10.1007/BF00193536

54. J. T. Overpeck, T. Webb III, I. C. Prentice, Quantitative interpretation of fossil pollen spectra: Dissimilarity coefficients and the method of modern analogs. *Quat. Res.* **23**, 87–108 (1985). doi:10.1016/0033-5894(85)90074-2

55. D. G. Gavin, W. W. Oswald, E. R. Wahl, J. W. Williams, A statistical approach to evaluating distance metrics and analog assignments for pollen records. *Quat. Res.* **60**, 356–367 (2003). doi:10.1016/S0033-5894(03)00088-7

56. G. L. Simpson, Modelling palaeoecological time series using Generalised Additive Models. *Front. Ecol. Evol.* **6**, 149 (2018). doi:10.3389/fevo.2018.00149

57. G. L. Simpson, H. Singmann, gratia: Graceful 'ggplot'-based graphics and other functions for GAMs fitted using 'mgcv' (2019); https://rdrr.io/cran/gratia/.

58. S. N. Wood, *Generalized Additive Models: An Introduction with R* (Chapman and Hall/CRC Press, ed. 2, 2017).

59. J. L. Blois, J. W. Williams, E. C. Grimm, S. T. Jackson, R. W. Graham, A methodological framework for assessing and reducing temporal uncertainty in paleovegetation mapping from late-Quaternary pollen records. *Quat. Sci. Rev.* **30**, 1926–1939 (2011). doi:10.1016/j.quascirev.2011.04.017

60. T. Giesecke, B. Davis, S. Brewer, W. Finsinger, S. Wolters, M. Blaauw, J.-L. de Beaulieu, H. Binney, R. M. Fyfe, M.-J. Gaillard, G. Gil-Romera, W. O. van der Knaap, P. Kuneš, N. Kühl, J. F. N. van Leeuwen, M. Leydet, A. F. Lotter, E. Ortu, M. Semmler, R. H. W. Bradshaw, Towards mapping the late Quaternary vegetation change of Europe. *Veg. Hist. Archaeobot.* **23**, 75–86 (2014). doi:10.1007/s00334-012-0390-y

61. S. G. A. Flantua, M. Blaauw, H. Hooghiemstra, Geochronological database and classification system for age uncertainties in Neotropical pollen records. *Clim. Past* **12**, 387–414 (2016). doi:10.5194/cp-12-387-2016

62. K. K. Goldewijk, A. Beusen, G. van Drecht, M. de Vos, The HYDE 3.1 spatially explicit database of human-induced global land-use change over the past 12,000 years. *Glob. Ecol. Biogeogr.* **20**, 73–86 (2011). doi:10.1111/j.1466-8238.2010.00587.x

63. J. H. McAndrews, in *Vegetation History*, B. Huntley, T. Webb, Eds., vol. 7 of *Handbook of Vegetation Science* (Springer, 1988), pp. 673–697.

64. J. H. McAndrews, Late Quaternary vegetation history of Rice Lake, Ontario, and the McIntyre archaeological site. *Archaeol. Surv. Can. Pap.* **26**, 161–189 (1984).

65. E. W. B. Russell, *People and the Land Through Time: Linking Ecology and History* (Yale Univ. Press, 1998).

66. S. E. Munoz, K. Gajewski, Distinguishing prehistoric human influence on late-Holocene forests in southern Ontario, Canada. *Holocene* **20**, 967–981 (2010). doi:10.1177/0959683610362815

67. S. E. Munoz, K. Gajewski, M. C. Peros, Synchronous environmental and cultural change in the prehistory of the northeastern United States. *Proc. Natl. Acad. Sci. U.S.A.* **107**, 22008–22013 (2010). doi:10.1073/pnas.1005764107 Medline

68. W. W. Oswald, D. R. Foster, B. N. Shuman, E. S. Chilton, D. L. Doucette, D. L. Duranleau, Conservation implications of limited Native American impacts in pre-contact New England. *Nat. Sustain.* **3**, 241–246 (2020). doi:10.1038/s41893-019-0466-0

69. C. I. Roos, Scale in the study of Indigenous burning. *Nat. Sustain.* **3**, 898–899 (2020). doi:10.1038/s41893-020-0579-5

70. J. Marsicek, B. N. Shuman, P. J. Bartlein, S. L. Shafer, S. Brewer, Reconciling divergent trends and millennial variations in Holocene temperatures. *Nature* **554**, 92–96 (2018). doi:10.1038/nature25464 Medline

71. N. Ramankutty, J. A. Foley, Estimating historical changes in land cover:North American croplands from 1850 to 1992. *Glob. Ecol. Biogeogr.* **8**, 381–396 (1999). doi:10.1046/j.1365-2699.1999.00141.x

72. T. M. Bonnicksen, America's ancient forests: From the ice age to the age of discovery. *Environ. Hist.* **5**, 567–568 (2000). doi:10.2307/3985594

73. S. T. Jackson, R. S. Webb, K. H. Anderson, J. T. Overpeck, T. Webb III, J. W. Williams, B. C. S. Hansen, Vegetation and environment in Eastern North America during the Last Glacial Maximum. *Quat. Sci. Rev.* **19**, 489–508 (2000). doi:10.1016/S0277-3791(99)00093-1

74. T. Giesecke, S. Brewer, W. Finsinger, M. Leydet, R. H. W. Bradshaw, Patterns and dynamics of European vegetation change over the last 15,000 years. *J. Biogeogr.* **44**, 1441–1456 (2017). doi:10.1111/jbi.12974

75. H. Binney, M. Edwards, M. Macias-Fauria, A. Lozhkin, P. Anderson, J. O. Kaplan, A. Andreev, E. Bezrukova, T. Blyakharchuk, V. Jankovska, I. Khazina, S. Krivonogov, K. Kremenetski, J. Nield, E. Novenko, N. Ryabogina, N. Solovieva, K. Willis, V. Zernitskaya, Vegetation of Eurasia from the last glacial maximum to present: Key biogeographic patterns. *Quat. Sci. Rev.* **157**, 80–97 (2017). doi:10.1016/j.quascirev.2016.11.022

76. L. Petherick, H. Bostock, T. J. Cohen, K. Fitzsimmons, J. Tibby, M.-S. Fletcher, P. Moss, J. Reeves, S. Mooney, T. Barrows, J. Kemp, J. Jansen, G. Nanson, A. Dosseto, Climatic records over the past 30 ka from temperate Australia – a synthesis from the Oz-INTIMATE workgroup. *Quat. Sci. Rev.* **74**, 58–77 (2013). doi:10.1016/j.quascirev.2012.12.012

77. H. Wu, J. Guiot, S. Brewer, Z. Guo, Climatic changes in Eurasia and Africa at the last glacial maximum and mid-Holocene: Reconstruction from pollen data using inverse vegetation modelling. *Clim. Dyn.* **29**, 211–229 (2007). doi:10.1007/s00382-007-0231-3

ERRATUM

Erratum for the Report “Global acceleration in rates of vegetation change over the past 18,000 years,” by O. Mottl, S. G. A. Flantua, K. P. Bhatta,V. A. Felde, T. Giesecke, S. Goring, E. C. Grimm, S. Haberle, H. Hooghiemstra, S. Ivory, P. Kuneš, S. Wolters, A. W. R. Seddon, J. W. Williams

+ See all authors and affiliations

Science 09 Jul 2021:
Vol. 373, Issue 6551, eabk222
DOI: 10.1126/science.abk2221

After publication of the Report “**Global acceleration in rates of vegetation change over the past 18,000 years**,” a bug was detected in the R-Ratepol code that affected the assignment of ages to individual time bins. The code should have assigned the average age estimate of the bin to each bin but instead assigned the average of the ages based on samples in that same bin. Correcting this error tends to further amplify Late Holocene rates of change relative to earlier periods while having no effect on the main conclusions drawn in the paper. Figures 2, 3, and 4 have been corrected, and reference 40 has been updated to direct readers to the corrected code. An alternative analysis with rates of change calculated only between adjacent time bins did not substantively differ from the corrected results. The authors thank R. Telford for drawing attention to these potential concerns. As-published and corrected code versions are available at **https://github.com/HOPE-UIB-BIO/Global_RoC** and **https://zenodo.org/record/4972077**.